



OPEN ACCESS

EDITED BY

Gang Rao,
Southwest Petroleum University, China

REVIEWED BY

Liang Qiu,
China University of Geosciences, China
Lei Wu,
Zhejiang University, China

*CORRESPONDENCE

Ahmad Rashidi,
✉ rashidi@uk.ac.ir
Reza Derakhshani,
✉ r.derakhshani@uu.nl

RECEIVED 19 February 2023

ACCEPTED 06 April 2023

PUBLISHED 05 May 2023

CITATION

Rashidi A, Shafieibafti S, Nemati M,
Ezati M, Gholami E, Mousavi SM and
Derakhshani R (2023), Flexural-slip
folding in buckling phases of orogenic
belts: Insight into the tectonic evolution
of fault splays in the East Iran orogen.
Front. Earth Sci. 11:1169667.
doi: 10.3389/feart.2023.1169667

COPYRIGHT

© 2023 Rashidi, Shafieibafti, Nemati,
Ezati, Gholami, Mousavi and Derakhshani.
This is an open-access article distributed
under the terms of the [Creative
Commons Attribution License \(CC BY\)](https://creativecommons.org/licenses/by/4.0/).
The use, distribution or reproduction in
other forums is permitted, provided the
original author(s) and the copyright
owner(s) are credited and that the original
publication in this journal is cited, in
accordance with accepted academic
practice. No use, distribution or
reproduction is permitted which does not
comply with these terms.

Flexural-slip folding in buckling phases of orogenic belts: Insight into the tectonic evolution of fault splays in the East Iran orogen

Ahmad Rashidi^{1,2*}, Shahram Shafieibafti³, Majid Nemati^{1,3},
Maryam Ezati⁴, Ebrahim Gholami⁴, Seyed Morteza Mousavi⁴ and
Reza Derakhshani^{3,5*}

¹Department of Earthquake Research, Shahid Bahonar University of Kerman, Kerman, Iran, ²Department of Seismotectonics, International Institute of Earthquake Engineering and Seismology, Tehran, Iran, ³Department of Geology, Shahid Bahonar University of Kerman, Kerman, Iran, ⁴Department of Geology, University of Birjand, Birjand, Iran, ⁵Department of Earth Sciences, Utrecht University, Utrecht, Netherlands

Introduction: The East Iran orogen has experienced multiple buckling phases resulting in the formation of strike-slip fault splays. The geometric and kinematic characteristics of these splays are influenced by folding mechanisms. This study focuses on investigating the structural characteristics and tectonic evolution model of the Khouf splay, located in the northern terminus of the Nehbandan right-lateral strike-slip fault system.

Methods: Field visits and geometrical properties from map views were used to analyze the structural features of the Khouf splay. The splay was found to consist of a multi-plunging anticline and syncline, referred to as the Khouf anticline and Khouf syncline, respectively. Flexural slip was identified as a significant mechanism for the formation of these structures. Structural evidence, including parasitic folds, active folds, and strike-slip duplexes, suggested that flexural slip occurred on discrete movement horizons among the rock units.

Results: Analysis of the parasitic folds in the cores and limbs of the Khouf anticline and syncline revealed M, W, Z, and S shapes, with complex slicken-line patterns observed on faults parallel to the beds at the limbs. The analysis results indicated strain partitioning and inclined left- and right-lateral transpressional zones. Shortening estimates obtained from profiles in the Shekarab inclined transpressional zone were approximately 33%, 65%, and 68% for NE-SW, N-S, and NW-SE profiles, respectively. In the Arc area, which is the core of the anticline, shortening estimates from NE-SW and N-S profiles ranged from 14% to 10%. Structural analysis of the folds in this area revealed broad, close, semi-elliptical, and parabolic shapes, suggesting that secondary folds with NW-SE axis directions have been superimposed on the first-generation folds with E-W axis directions in the Khouf refolded splay.

Discussion: The findings of this study highlight the structural characteristics and tectonic evolution model of the Khouf splay in the northern terminus of the Nehbandan right-lateral strike-slip fault system. The results suggest that flexural slip played a crucial role in the formation of the multi-plunging anticline and syncline in the Khouf splay. The presence of parasitic folds and complex slicken-line patterns on faults indicate the complexity of deformation processes. The

observed strain partitioning and inclined transpressional zones suggest a complex tectonic history in the study area. The superimposition of secondary folds with different axis directions on first-generation folds adds further complexity to the structural evolution of the Khouf refolded splay. Overall, this study provides new insights into the structural characteristics and tectonic evolution of the Khouf splay in the East Iran orogen.

KEYWORDS

structural geology, parasitic folds, strain, shortening estimation, refolding, inclined transpression

1 Introduction

Displacement models of the fold formations have been extensively studied through laboratory experiments and the simple card method (e.g., Shiells, 1963; Hibbard et al., 2004). The mathematical analysis of fold geometry, specifically the strain matrix, determines the overall strain field in the folded layers. The strains in various types of buckle folds are examined using the models of flexural-flow, flexural-slip, tangential longitudinal strain, inverse tangential longitudinal strain, and the effects of prefold strains arising from initial compaction, parallel layer shortening, and oblique early tectonic strains (Twiss and Moores, 2007; Fossen, 2016; Ghanbarian et al., 2021). The development of small-scale structural features in different parts of a fold depends on the large-scale fold geometry with a specific mechanism (Davis, 2014; Ghanbarian and Derakhshani, 2022a). The significance of slipping of folding layers has been investigated to provide valuable information about the large-scale tectonic structure and tectonic evolution model of the geological structures (Geoff Tanner, 1989; Ghanbarian and Derakhshani, 2022b).

In strike-slip faults terminations, the displacements are distributed through several branching splay faults. Synthetic and antithetic splay faults at the terminal tips of strike-slip faults usually have a vertical component consistent with the compressional or extensional character of the fault termination. The compressional horsetail splays can present thrust faults and folds at strike slip faults tips (Kim et al., 2004). The multiple buckling phases of orogenic belts during different geologic periods can form the refolding features in various scales within the compressional fault splay (Ghosh et al., 1993). One of the unique regions on the Earth's surface, which includes large-scale compressional splays, is known as the East Iran orogen region (Rashidi et al., 2022c) within the framework of the Alpine-Himalaya orogenic system (Figure 1).

Geodynamics of structural subzones of the Iranian plate, which located in the Alpine-Himalaya orogenic belt, are dependent on the convergence of the Arabian plate with the Eurasian plate (Jackson and McKenzie, 1984) (Figure 1A). Its major structural subzones include Central Iran (CI), the NW-SE Zagros orogenic belt (Kamali et al., 2023) to the southwest, the E-W Makran (Ma) to the southeast, the E-W Alborz (AM)-Kopeh Dagh (KD) to the north, and the N-S Eastern Iran orogen (EOI) (Ezati et al., 2022a; 2022b) to the east of Iran (Figure 1B). The dominating crustal deformation in the East Iran orogen (EOI) and Central Iran (CI) (including the Lut (LB), Tabas (Ta), and Yazd (Ya) crustal blocks) are accommodated by

crustal shortening and vertical axis fault-block rotations (Walker and Khatib, 2006) and control the present kinematics of them.

The N-S Nehbandan right-lateral strike-slip fault system with a length of ~600 km, which includes two west Neh (W.F.) and east Neh (E.F.) branches, overprints Eastern Iran orogen (EOI) and separates the Lut block (LB) from the Afghan block (AB) (Figure 1B) (Şengör et al., 1988). The northern terminal of the fault ends in the E-W and NW-SE faults (Walker and Khatib, 2006), where the most dominant splays, including Khouf, Birjand, Sedeh, Abiz, Nowzad, Hashtoogan, and Qaryan (Figure 1C). According to the rheology of the splays rock units, their deformation type can be generally divided into two categories: brittle and ductile deformation.

The Birjand splay, with its brittle characteristics, separates the Tertiary ophiolite rock units from the Quaternary alluvial covers to the north and south (Walker and Khatib, 2006). The kinematic of the Birjand splay has been controlled by dominant N-S right-lateral strike-slip, NW-SE oblique, and E-W left-lateral strike-slip faults. The western part of the Splay follows the left-lateral transpressional model, and its eastern part follows the push-up structures at the N-S strike-slip stepovers (Rashidi et al., 2022c).

The Khouf splay in the north of Birjand, a part of the old isolated splay or a part of the Qaen allochthonous belt (Bagheri and Damani Gol, 2020), includes more ductile deformation. Its rock units are mostly sedimentary and volcano-sedimentary. Folds with different geometries and axial-trace directions, parasitic folds (or passive flow folding), shear duplexes, and faults parallel to the beds are the essential features of the splay. In the Khouf splay (as a large-scale refolded platform), due to different buckling phases of the East Iran orogen, a series of secondary folds had been superimposed on the previous folds. In this research, to determine the tectonic evolution model of the Khouf splay (as a ductile splay in the East Iran orogen), we investigated the geometric-kinematic relationship of the small-scale structural features with the large-scale refolded platform. A combination of structural cross-sections and their balance, amount of crustal shortening, current, and paleo-stress were required to achieve this goal. We specifically selected two areas "Arc" and "Shekarab," within Khouf splay to calculate the crustal shortening and determine the geometry of the fold using different geometric methods. We investigated the folding mechanisms in these areas and all over the Khouf splay as an essential factor in the formation of geological structures and presented a new tectonic evolution model of the small and large-scales features.

This study presents new data on the identification of folds, faults, and their mechanism, and the fusion of multiple buckling phases of

East Iran orogen with the field and satellite data in order to investigate the structural characteristic of the north part of the East Iran orogen in the framework of the Eurasia-India and Arabia convergence. Therefore, our aims in this research are to decipher: (i) how folds superimposed on each other during the buckling phases of the East Iran orogenic; (ii) how N-S right-lateral shearing between the Lut block and Afghan block, and E-W left-lateral shearing within the Eastern Iran orogen (EOI) have been accommodated through large/small scale refolding in the compressional terminus of the strike-slip faults, and (iii) role of fold mechanisms in the tectonic configuration and geometric and kinematic analysis of orogenic belts.

2 Tectonic setting

The Iranian plateau, one of the important sub-plateaus of the Alpine-Himalaya orogenic belt, has formed due to the progressive closure of the Tethys oceans and the continental collisions (Stocklin, 1968; Derakhshani and Farhoudi, 2005; Qiu et al., 2016; 2022). The northern mountain ranges of the Iranian plateau (e.g., E-W Alborz and Kopeh-Dagh ranges) were the results of different tectonic occurrences from the late Triassic Cimmerian orogeny to the current-day stage of intra-continental deformation resulting from the Arabian- Eurasian convergence (Sengoer, 1979; Berberian and King, 1981; Şengör, 1984). The

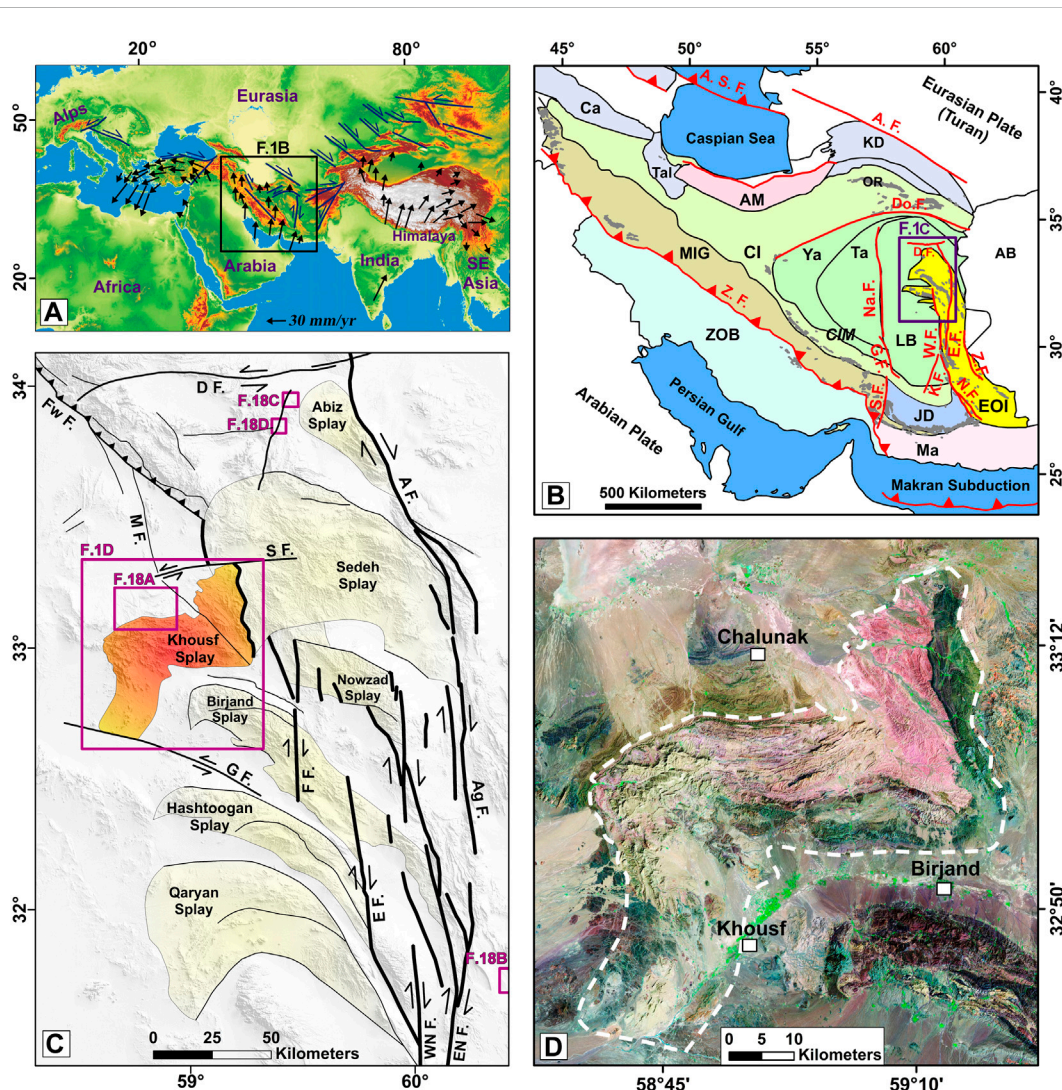


FIGURE 1

Tectonic position of the study area. (A) The SRTM30 map of the Alpine-Himalaya orogenic system resulted from the convergence of the Eurasian plate with the African, Arabian, and Indian plates. The velocities vectors of the GPS are relative to the Eurasian reference frame (Vernant et al., 2004). (B) The regional structures of the Arabia- Eurasia convergence and the position of the Eastern Iran orogen. Abbreviations: EOI = Eastern Iran orogen; Ca = Caucasus; KD = Kopet Dagh; AM = Alborz Mountains; Tal = Talesh; MIG = zone of metamorphic rocks and intruded granitoides; CIM= Central Iranian Microcontinent; Ta = Tabas; Ya = Yazd; CI = Central Iran; AB = Afghan block; LB = Lut block; ZOB = Zagros orogenic belt; Ma = Makran; JD = Jazmurian depression; OR = ophiolitic rocks; E F. = East Neh fault; W. F. = West Neh fault; N. F. = Nosratabad fault K. F. = Kahourak fault; Z. F. = Zahedan fault; D. F. = Dasht-e Bayaz fault; Do. F. = Doruneh fault; S.F. = Sabzevaran fault; G.F. = Gowk fault; Na.F. = Nayband fault; A.F. = Ashkabad fault; A.S.F. = Apsheeron Sill fault. (C) The compressional splays of the right-lateral faults termination in the northern part of the East Iran orogen. D. F. = Dasht-e Bayaz fault; AF = Abiz fault; S. F. = Sedeh fault; Fw F. = Ferdows fault; Ag F. = Abegarm fault; EN F. = East Neh fault; WN F. = West Neh fault; E. F. = Esmailabad fault; FF = Fanud fault. (D) Close-up view of the Khouf splay (or Khouf folded platform). See its geological details in Figure 2.

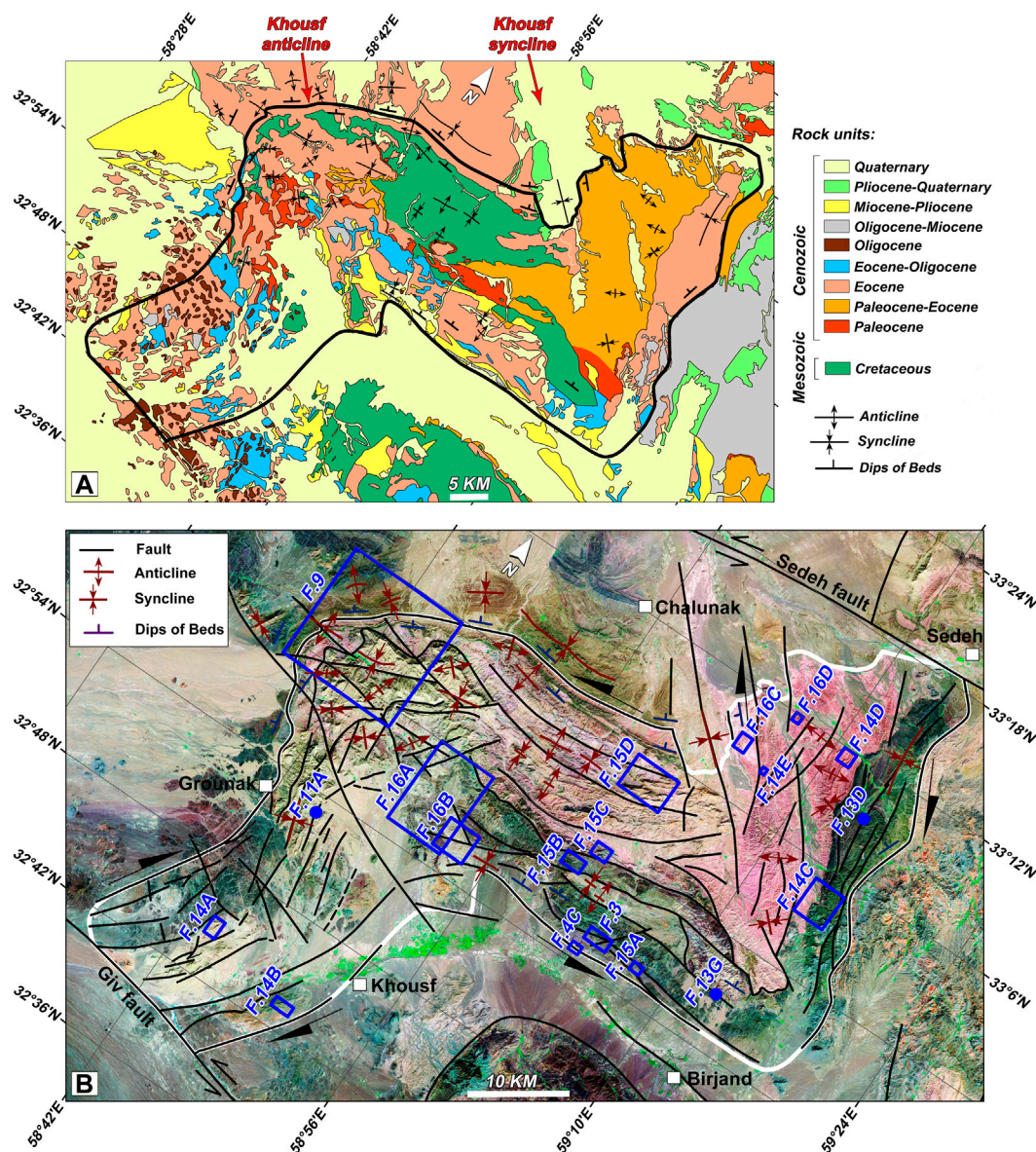


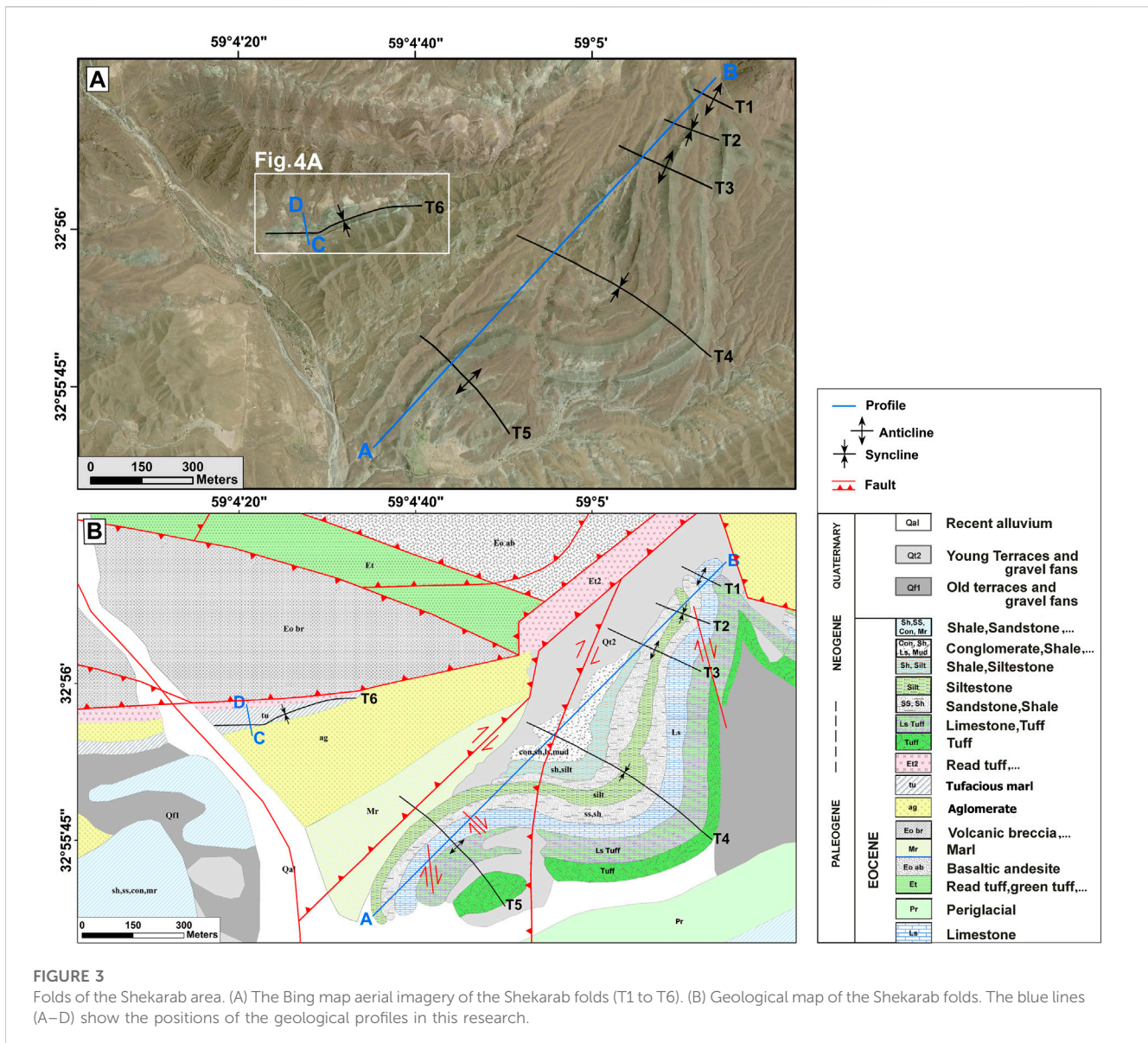
FIGURE 2

Geological and structural map of the Khouf folded platform. (A) Geological map of the area. The black polygon shows the position of the Khouf folded platform, which includes the Khouf anticline and syncline. (B) Structural map of the folded platform. White and blue polygons show the position of the folded platform and the following figures, respectively.

Cimmerian orogeny, which has affected the Eurasian margin from Turkey to Thailand, has been caused due to the early Mesozoic collision of some micro-plates separated from the Gondwana continent (Stocklin, 1974; Stampfli et al., 1991). From the late Cretaceous to the Paleocene, tectonic movements dependent on the Laramide orogeny, leading to a compressional mechanism, has occurred along the ranges, marked by the faulting and the folding of Cretaceous to Paleocene rock units (Stocklin, 1974). In the northern part of the ranges, marine deposition of Paleocene is visible, while no sign of Eocene rock units was seen. However, relics of reworked Eocene fauna in younger rock units show that Eocene rocks were

eroded after the onset of orogenic uplift in the Oligocene (Ghassemi, 1990), such as Pyrenean orogenic.

The southern mountain ranges of the Iranian plateau (e.g., NW-SE Zagros and E-W Makran ranges) were formed due to the subduction of the Neotethyan oceanic crust beneath Central Iran after the late Jurassic, which is still active in the Makran area (Derakhshani et al., 2023). In the N-S eastern mountain range of the Iranian plateau, the Sistan suture zone (Freund, 1970) has resulted from the closing of the Sistan ocean (Camp and Griffis, 1982) as a back-arc zone of the Neotethyan oceanic domain in the late Cretaceous (Berberian and Berberian, 1981). The geochemical characteristics of the post-late Cretaceous rock



units are generally consistent with this geodynamic scenario. Currently, East Iran's orogen follows a curved pattern to the east and west in its southern and northern domains, respectively (Figure 1B). This orogenic belt which is located between the Afghan block in the east and sub-zones of Central Iran (e.g., the Lut block) in the west includes the fastest-slipping faults in eastern Iran (Figure 1B) (Walker and Khatib, 2006; Mehrabi et al., 2021; Rashidi et al., 2021). The Nehbandan (West Neh and East Neh branches), Nosrat-Abad and Kahourak faults within the East Iran orogen constitute the eastern boundary of the Lut block, and the Sabzevaran, Gowk, and Nayband faults determine the western boundary of the Lut block (Figure 1B) (Hashemi et al., 2018; Rashidi et al., 2020). These active faults are laterally slipping at a rate of 5.6 ± 0.6 mm/yr and 4.4 ± 0.4 mm/yr, respectively (Walpersdorf et al., 2014). The maximum stress direction (σ_1) in the East Iran orogen was determined by the weighted average of the focal mechanism stress inversion, seismic strain rate, and

geodetic strain rate at about N36°E (Nemati and Derakhshani, 2021; Rashidi et al., 2022b). This stress direction is positively correlated with the current mechanism of the faults in the area so that the NS and EW faults, respectively, display dominant right-lateral and left-lateral movements, and the NW-SE faults indicate the reverse movement (Walker and Khatib, 2006; Rashidi et al., 2022c). Some of these faults caused destructive earthquakes such as the Mw 7.2, 1997, Zirkuh (Berberian et al., 1999), the Mw 7.1, 1968, west Dasht-e Bayaz (Ambraseys and Tchalenko, 1969), the Mw 7.1, 1979, Khuli-Boniabad (Nowroozi and Mohajer-Ashjai, 1980), and the Mw 6.2, 1968, Ferdows (Walker et al., 2003).

The East Iran orogen displays some splays of shear and thrust sheets with rocks of different origins (Camp and Griffis, 1982). The Cenozoic volcanic to subvolcanic rocks that have been mildly deformed are emplaced on the orogenic belt surrounding the region. The sedimentary basins of eastern Iran were elongated basins filled with a large volume of turbiditic and pelagic

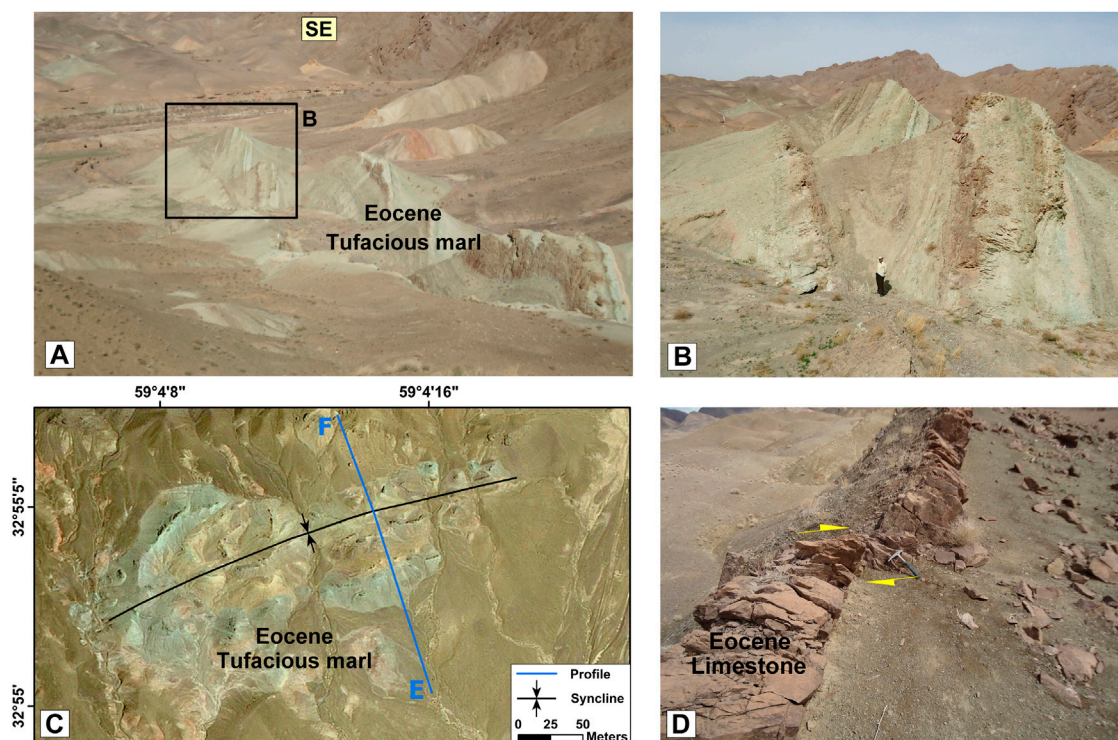


FIGURE 4

T6 and T7 fold in the Shekarab area with an example of displacement in the folded layers. (A) Field images of the T6 syncline. (B) Close-up view of the syncline. (C) The Bing map aerial imagery of the T7 syncline with the position of the ~NW-SE profile. See the figure location in Figure 2B. (D) Field image of a displacement in the folded layers by the minor strike-slip fault.

sediments (Tirrul et al., 1983), called the flysch zone of east Iran (Eftekharneshad, 1980).

The northern domain of the Sistan orogenic belt had been considered as accretionary prisms, including two late Cretaceous-lower Eocene ophiolitic complexes of Neh and Ratuk with the sediment deposits of the Sefidabeh forearc basin (Tirrul et al., 1983). The Sefidabeh basin includes clastic sediments with episodes of carbonate sediments and calc-alkaline volcanism. The Sefidabeh basin and its basement were severely deformed by post-late Cretaceous faulting and folding (Tirrul et al., 1983). This research focused on the northern domain of the East Iran orogen (Khouf splay) in the north-northwest of the Birjand, with mostly folded sedimentary and volcanic deposits (Figure 2).

3 Data and methodology

To investigate the post-Cretaceous tectonic evolution model of the Khouf folded platform (Khouf splay) and its smaller-scale structural features, we employed an integrated approach that combined field evidence with satellite image analysis. During field visits, the geometric and kinematic characteristics of the faults, such as the orientation of the faults and their slickenlines, and the attitude of the rock units, including strike, dip, and dip direction, were carefully determined (Federico et al., 2014). The data

was collected using classical methodologies, such as the use of a compass, goniometer, and tiltmeter.

The flexural slip, which is a mechanism for the formation of some faults (e.g., strike-slip faults) and folds (e.g., chevron, parallel folds), involves the interlayer sliding towards the anticlinal and synclinal axes during the folding (van Hise and Hoskins, 1896; Leith, 1923). According to the sliding direction on the fold limbs, flexing of the beds can create parasitic folds (or flexural flow folding) within each bed of the flexural slip fold (Cloos and Martin, 1932). In the field visits of the large-scale Khouf folded platform, we examined the interlayer sliding surfaces amount of slip on each surface, and we investigated the parasitic folds on the satellite images.

In order to conduct a structural analysis of the area, we prepared some new detailed structural and geological maps. To evaluate the tectonic shortening resulting from pressure and shear on the limbs and cores of the Khouf folded platform, some NW-SE, N-S, and NE-SW geological profiles and their restoration was prepared. Profiles were restored between two pinning lines. The layers in the profiles are continuous, and there are no gaps or overlaps between the restored layers. We benefited from the various studies which have been done on the method details of how to restore geological profiles (Behrmann et al., 1991; Espurt et al., 2019). The shortening along the profiles is calculated by the length of the restored and deformed profiles (L0-Ld). Shortening ratios were also measured in percent to compare the relative shortening of the profiles which don't have the same length and direction.

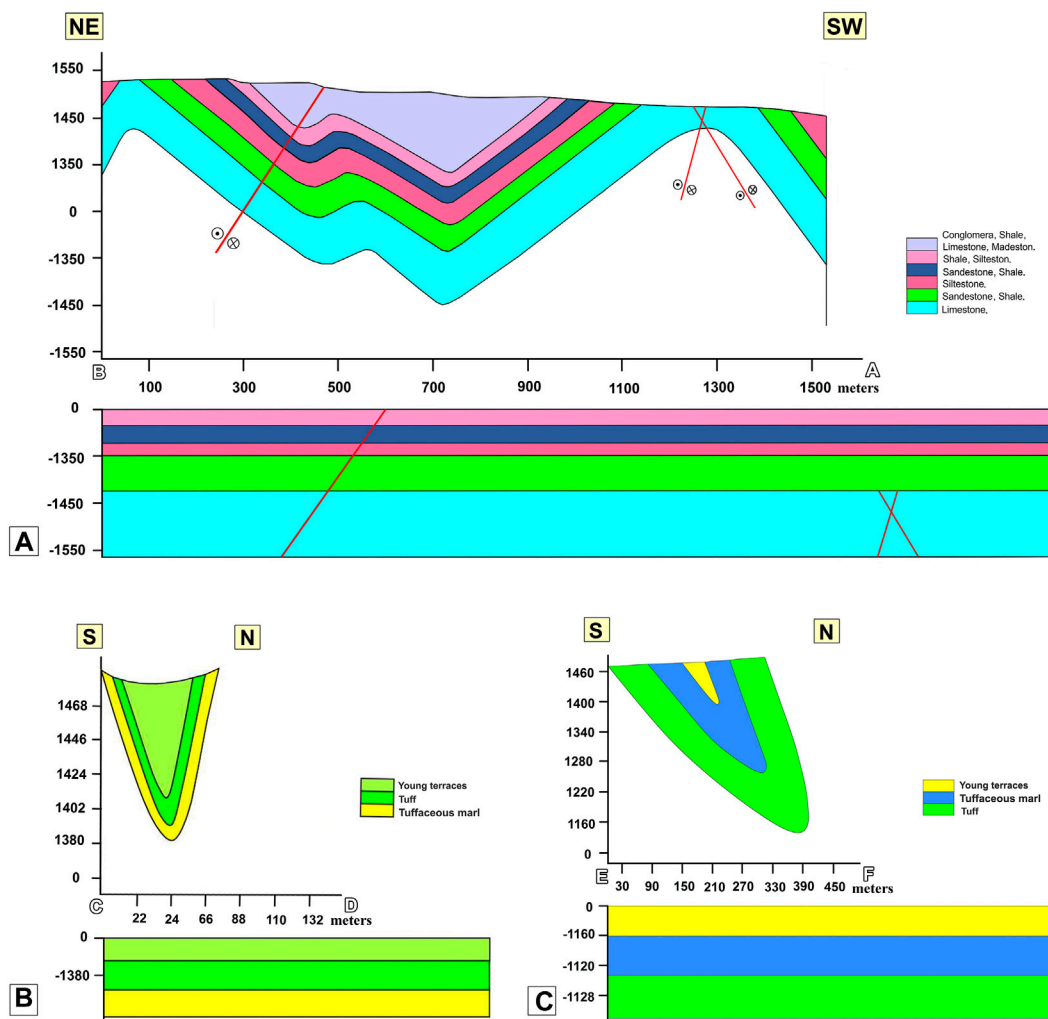


FIGURE 5 Geological profiles depicting the restored T1 to T5, T6, and T7 folds in the Shekarab area. (A) Profile A-B pertains to the T1 to T5 folds, and its location can be found in Figure 3. (B) Profile C-D represents the T6 fold, and its position is indicated in Figure 3. (C) Profile E-F relates to the T7 fold, and its location can be seen in Figure 4C.

TABLE 1 Geometric properties of the T1 to T7 folds in the Shekarab area. Abbreviations: A_+ = amplitude (meter); M_+ = wavelength (meter); P = aspect ratio; r = interlimb angle (degree); b = fold bluntness; b_1 , b_3 = Fourier coefficients.

Fold name	A (m)	M (m)	P	Fold style	r (degree)	Tightness	b	b1	b3	Fold shape	Amplitude number
T1	195	335	1.16	Equant	68	Close	0.24	-0.19	3.9	Sine waves-Chevron	3-4
T2	210	120	3.5	Short	54	Close	0.38	0.06	4.5	Sine waves- Parabolas	3-4
T3	221	190	2.33	Short	80	Open	0.29	0.03	4.1	Sine waves- Parabolas	3-4
T4	370	300	2.47	Short	116	Open	0.21	0.64	7.6	Semi-ellipses, Parabolas	4-5
T5	320	550	1.16	Equant	136	Gentle	0.13	0.68	4.5	Semi-ellipses	3-4
T6	66	75	1.76	Short	30	Tight	0.20	-0.34	7.8	Chevron	4-5
T7	175	325	1.08	Equant	30	Tight	0.17	-0.30	9.1	Chevron	4-5

TABLE 2 The position of some geometric-kinematic elements of the T1 to T7 folds in the Shekarab area. Abbreviations: A-P = Axial plane; H-P = Hinge point. σ_1 , σ_2 , σ_3 are, respectively, the maximum, medium, and minimum stress axis.

Fold name	A-P	Dip of A-P	H-P	Plunge of H-P	σ_1	σ_2	σ_3
T1	091,89	Upright	272,43	Moderately plunging	181,01	272,43	091,42
T2	291,80	Upright	288,21	Gently plunging	020,05	288,21	123,68
T3	302,76	Steeply inclined	295,34	Moderately plunging	033,12	295,34	139,53
T4	313,74	Steeply inclined	316,14	Gently plunging	222,17	316,14	085,67
T5	332,74	Steeply inclined	336,18	Gently plunging	243,12	336,18	120,67
T6	094,80	Upright	093,14	Gently plunging	184,03	093,14	286,75
T7	266,56	Moderately inclined	274,13	Gently plunging	175,35	274,13	021,52

TABLE 3 Geometric properties of the Fo1, Fo2, and Fo3 fold in the Arc area. Abbreviations: A = amplitude (meter); M = wavelength (meter); P = aspect ratio; r = interlimb angle (degree); b = fold bluntness; b1, b3 = Fourier coefficients.

Fold name	A (m)	M (m)	P	Fold style	r (degree)	Tightness	b	b1	b3	Fold shape	Amplitude number
Fo1	258	1,382	0.37	Broad	74	Open	0.98	9.82	0.88	Semi-ellipses, Parabolas	4-5
Fo2	161	564	0.57	Broad	53	Close	0.94	8.14	0.73	Semi-ellipses, Parabolas	4-5
Fo3	369	3218	0.23	Wide	122	Gentle	0.8	4.2	0.6	Semi-ellipses	3-4

The structural analysis of the main folds in the Shekarab and Arc areas was done by the fold geometry classification, which includes the aspect ratio (P), interlimb angle (r), fold bluntness (b), Fourier coefficients (b1, b3), fold shapes, tightness, and amplitude numbers definition. In this research, based on the Fleuty classification, the interlimb angles of the main folds were measured and divided into isoclinal (0 to 3°), tight (3° to 30°), close (30° to 70°), open (70° to 120°), and gentle (120°-180°). The following equation (Eq. 1) was used to determine the fold style in the Shekarab and Arc areas.

$$P = A/(M/2) \quad (1)$$

where A is fold amplitude and M is folds wavelength. Therefore, the aspect ratio (P) is defined as the ratio between the amplitude and half-wavelength of the folds (Hansen, 1971).

The fold bluntness (b) is the measurement of the roundness or angularity of the fold limbs. The fold bluntness (b; Eq. 2) is defined as the ratio of the curvature radius at the fold closure (rc) to the curvature radius of the reference circle (ro) (Twiss, 1988).

$$b = \begin{cases} \frac{rc}{ro} & \text{for } rc \leq ro \\ 2 - \frac{ro}{rc} & \text{for } rc \geq ro \end{cases} \quad (2)$$

The Fourier coefficients (b1 and b3), unique to each waveform (Stabler, 1968), are considered important inputs in describing the fold shapes. The principle amplitude of the folds is taken from the b1; however, these are modified by the b3. The b1 and b3 values (Eqs 3, 4) allow a mathematical classification of the folds profile. The Fourier transform for folds has been suggested by Hudleston and Stephansson (1973) to categorize the shapes of a profile

related to the folded surfaces through a graphical demonstration of b1 vs. b3, where just two coefficients, b1 and b3, of a sine series, are used:

$$b1 = \frac{y1 + \sqrt{3}y2 + y3}{3} \quad (3)$$

$$b3 = \frac{(2y1 - y3)}{3} \quad (4)$$

where y is the y-axis value of a fold located on the horizontal axis, and the y-axis is chosen to pass through the inflection point perpendicular to the y-axis where the origin is the inflection point (Stabler, 1968; Hudleston and Stephansson, 1973). The harmonic analysis or Fourier transform classifies folds into six standard shapes, which include A (box fold), B (between box folds and semi-ellipses), C (semi-ellipses), D (parabolas), E (between sine waves and chevron folds), and F (chevron folds) with five standard amplitude numbers (from 1 to 5) (Hudleston and Stephansson, 1973).

For a comprehensive tectonic analysis of the study area, a combination of structural and current/paleo-stress is required (Rashidi and Derakhshani, 2022). Therefore, we used stress data from recently published articles by some authors (Jentzer et al., 2017; Ezati et al., 2022b). The Tensor software (Delvaux et al., 1997; Delvaux et al., 2012; Delvaux and Sperner, 2003) was applied to illustrate the structural data, especially for the faults with slickenlines.

4 Results

Large-scale Khouf folded platform includes an anticline and a syncline (we named them Khouf anticline and Khouf syncline;

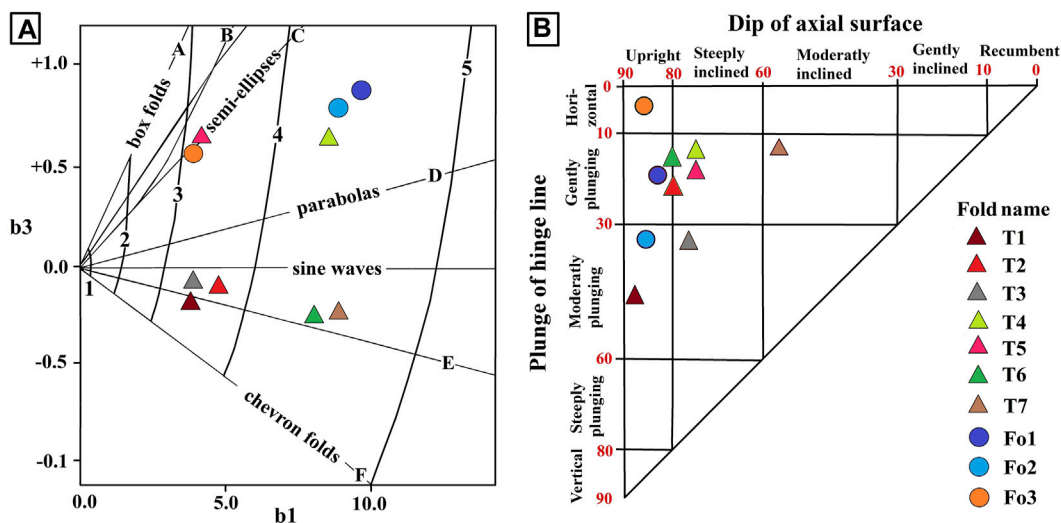


FIGURE 6

Diagrams of the (Fleuty, 1964; Hudleston and Stephansson, 1973) to determine the geometry classification of the folds in area. (A) Positions of the Shekarab and Arc folds on the (Hudleston and Stephansson, 1973) diagram based on the Fourier coefficients. (B) Positions of the Shekarab and Arc folds on the Fleuty (1964) diagram based on the dip of the axial surface and plunge of the hinge line. The colored triangles are the folds of the Shekarab area (T1 to T7), and the colored circles are the folds of the Arc region (Fo1, Fo2, and Fo3). See the characteristics of arc folds in Section 4.2. "Structural style of the Arc area".

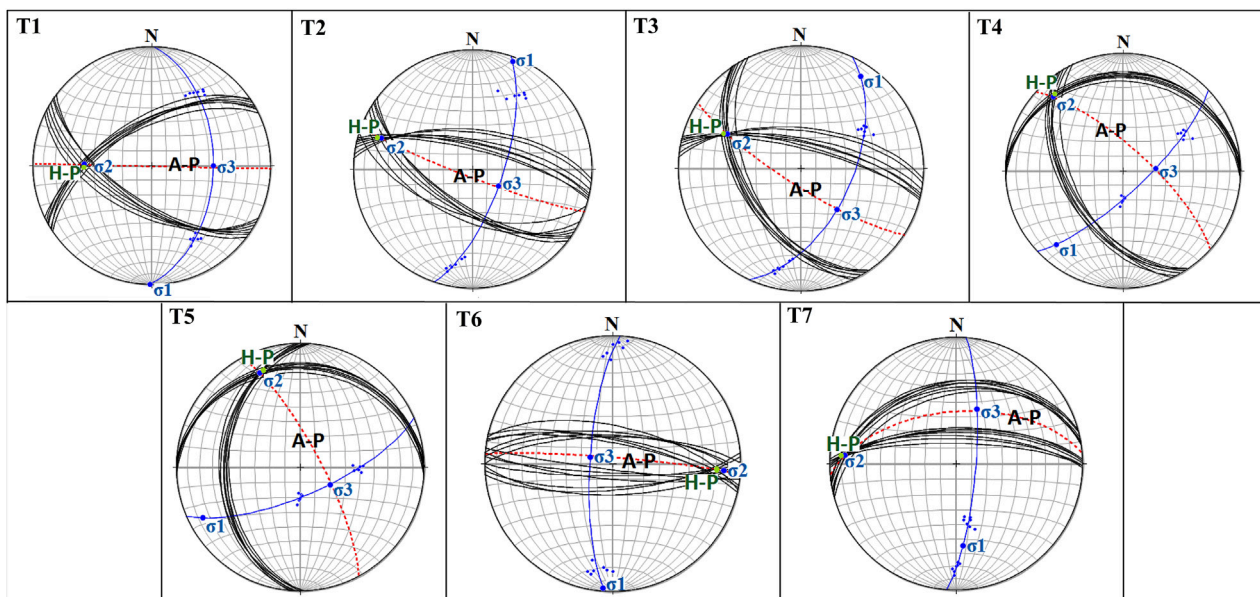


FIGURE 7

The geometric characteristic of the T1 to T7 folds on the Wulff net with their contour diagram and principal stress axes (σ_1 , σ_2 , σ_3). A-P= Axial plane; H-P= Hinge point.

Figure 2), and its modern geometry had been the result of various buckling phases of the East Iran orogen. Changes in stress directions have caused the creation of several generations of folding in the platform. In order to conduct a structural analysis of the folding process in the area, in the following, we investigated the structural

style of the Shekarab folds at the common limb of the anticline and syncline (F.5 and F.6c in Figure 2) and the Arc folds at the core of the anticline (F.11 on Figure 2). Then, we obtained kinematic and geometric characteristics of the small-scale geological structures (e.g., parasitic folds) in the Khusf folded platform.

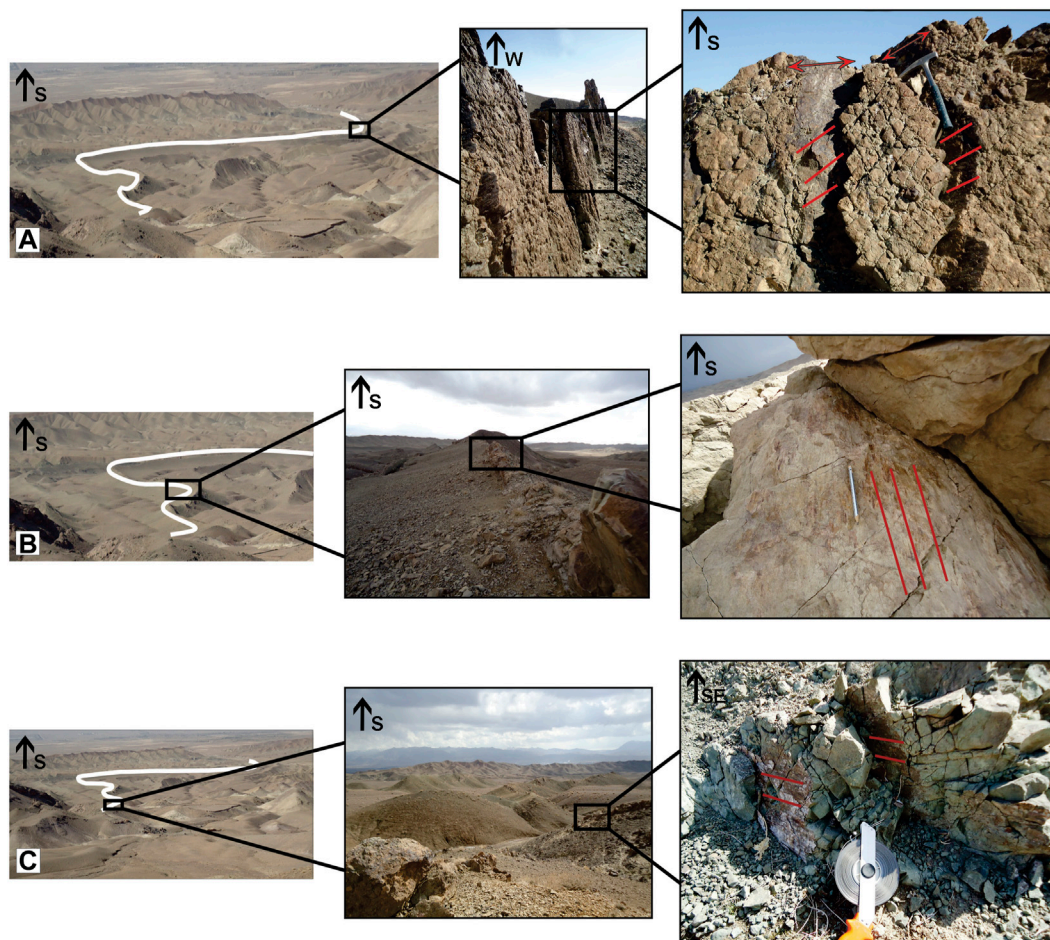


FIGURE 8

Examples of interlayer slips within the T1 to T5 folds result from the flexural-slip mechanism. (A) Interlayers slip in the T5 anticline. (B) Interlayers slip in the T3 anticline. (C) Interlayers slip in the T1 syncline.

4.1 Structural style of the Shekarab area

A transpressional zone has been introduced in a part of the common limbs of the Khousf anticline and syncline, which is known as the Shekarab area (Rashidi et al., 2022c). The lower and upper boundaries of this zone are the North Birjand fault and the Shekarab fault, respectively. These faults include several fault planes with different mechanisms (e.g., strike-slip, dip-slip, and oblique-slip) parallel to the rock units (Walker and Khatib, 2006). Within the Shekarab transpressional zone, the various geological structures, such as folds with different axial-trace directions, were formed during the progressive deformation (T1 to T6 in Figure 3A; T7 in Figures 4A,B).

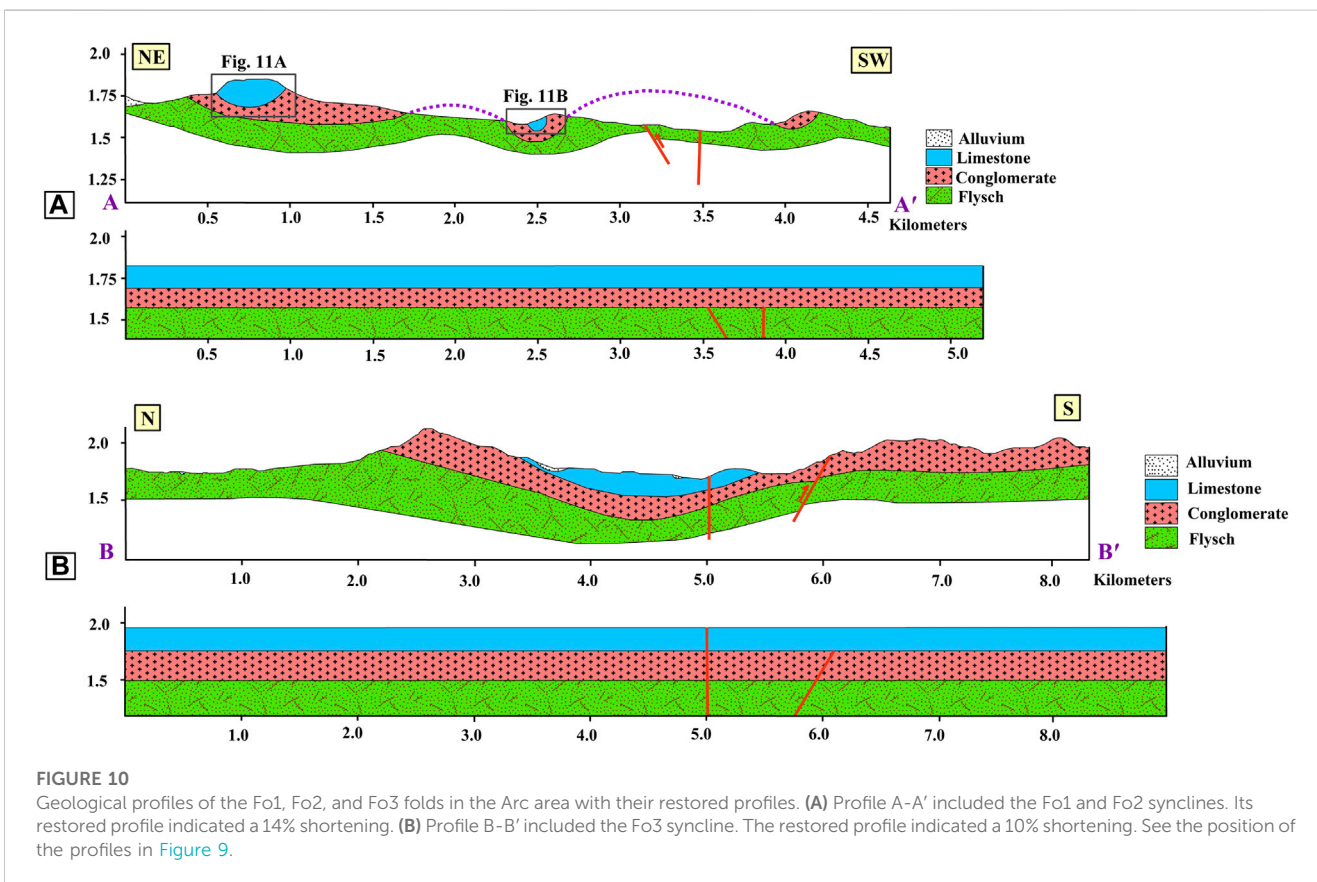
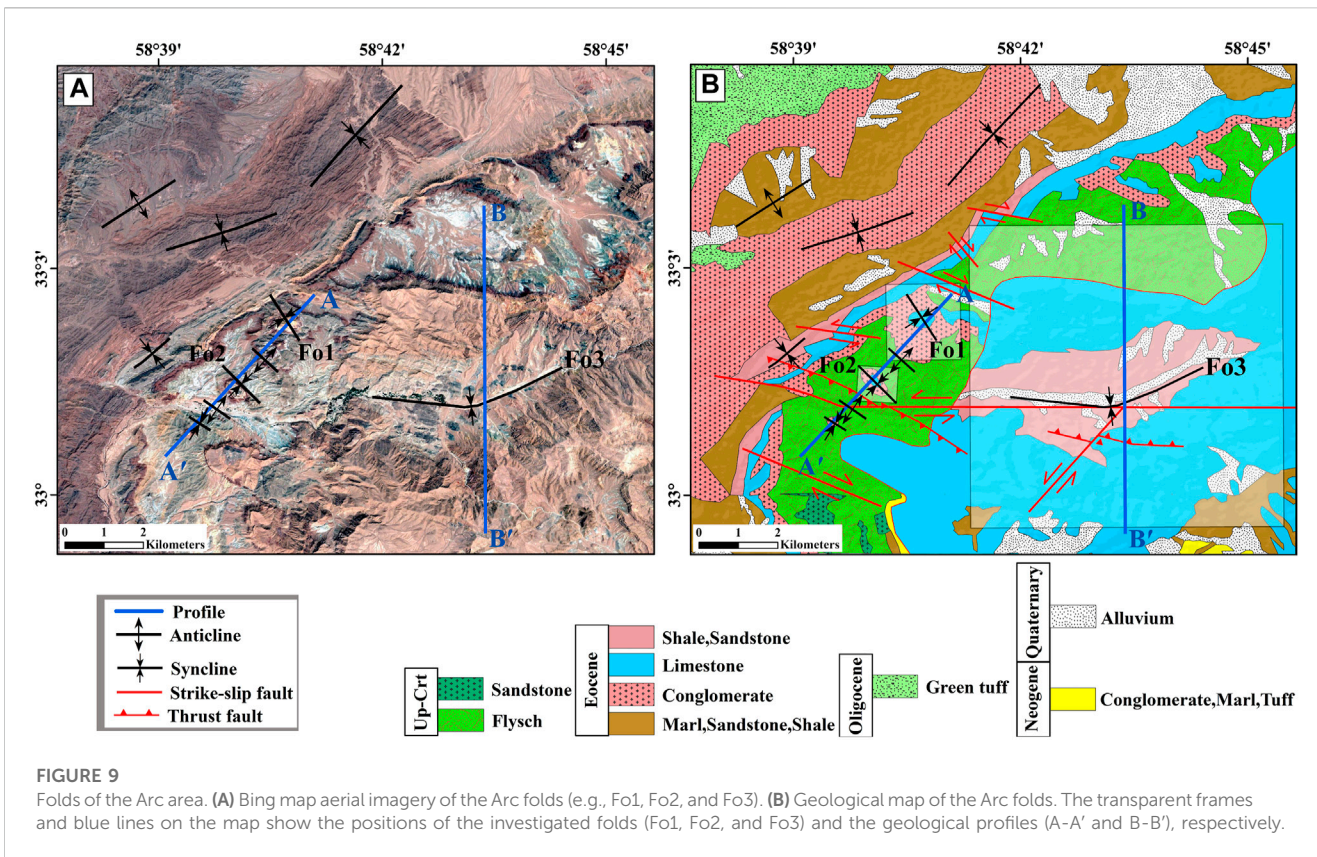
We obtained three geological profiles with different directions on the T1 to T5, T6, and T7 folds (Figures 3, 4C). The restored profiles were used to determine the fold geometry and amounts of shortening. Some faults had caused displacement in the Eocene sedimentary layers of the T1-T5 plunging folds (e.g., Figure 4D). To obtain the restored profile and calculate the amount of shortening, we eliminated the displacements and the plunges of the folds. Our

measurements indicated ~33% shortening in the NE-SW direction along the A-B profile (Figure 5A).

The C-D profile on the T6 fold (Figure 3B) follows the Eocene tuff and tuffaceous marl. The C-D restored profile indicated ~65% shortening in the N-S direction (Figure 5B). Along the E-F profile (Figure 4C), the Eocene tuffaceous marl and tuff are exposed on the ground surface. The restored profile on the T7 fold included ~68% shortening in the ~NW-SE direction (Figure 5C).

We present the folds geometry classification (e.g., aspect ratio, interlimb angle, fold bluntness, Fourier coefficients, fold shapes, tightness, and amplitude numbers definition) for the structural analysis in the area (Tables 1, 3).

The T1, T3, and T5 folds are asymmetric anticlines, and the T2, T4, and T6 folds are asymmetric synclines. The T7 fold is an overturned syncline, with attitude of the limbs as N65°E, 60°NW and N65°E, 70°NW. The T1 to T7 folds which are developed in the Shekarab transpressional zone have different axial-trace directions. Based on the fold geometry classification, the T1 fold is between sine waves and chevron folds; T2 and T3 are between sine waves and parabolas; T4 is between semi-ellipses and Parabolas; T5 is semi-



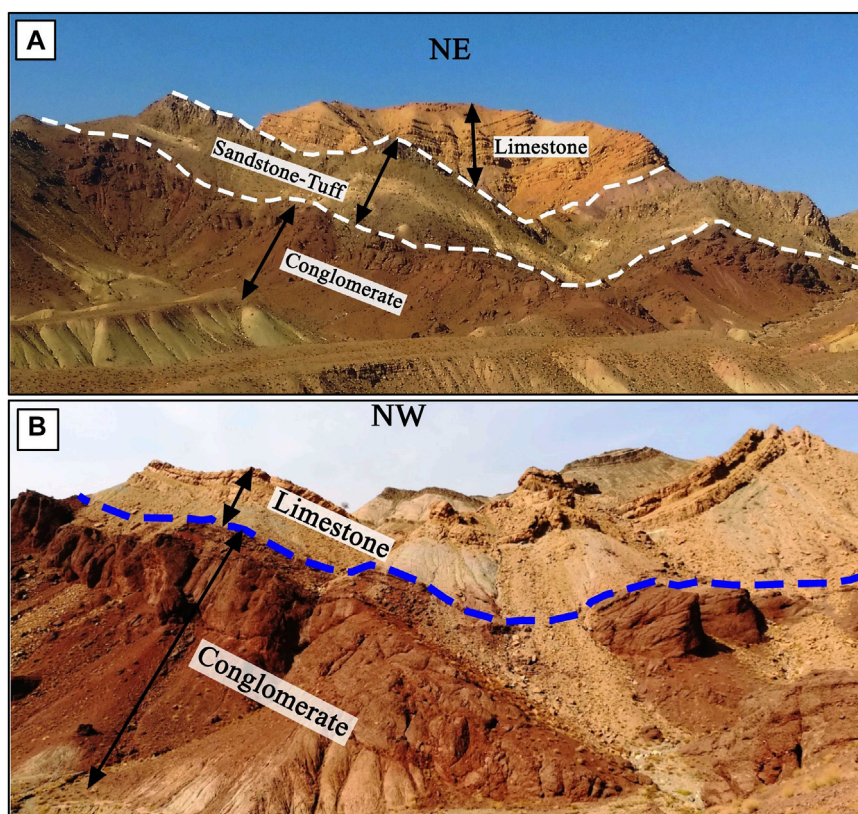


FIGURE 11
Field images of the folds (Fo1 and Fo2) within the post-Cretaceous flysch units. (A) The Fo1 syncline with ~55° and ~45° dips of the strata on the northwestern limb and southeastern limb, respectively. (B) The Fo2 syncline with ~60° and ~40° dips of the strata on the northwestern limb and southeastern limb, respectively.

TABLE 4 Geometric-kinematic positions of the Fo1, Fo2, and Fo3 folds in the Arc area. Abbreviations: A-P = Axial plane; H-P = Hinge point. σ_1 , σ_2 , σ_3 are, respectively, the maximum, medium, and minimum stress axis.

Fold name	A-P	Dip of A-P	H-P	Plunge of H-P	σ_1	σ_2	σ_3
Fo1	301,81	upright	299,15	Gently plunging	207,06	299,15	094,73
Fo2	145,85	upright	148,33	Moderately plunging	055,05	148,33	318,56
Fo3	088,86	upright	269,05	horizontal	179,04	269,05	060,83

ellipses, and T6 and T7 are chevron folds (Table 1; Figure 6). In Ramsay’s dip isogons categories (Ramsay J. G., 1967; Ramsay J. G., 1967), these folds are located in the class (1B). Based on the tightness classification, only T6 and T7 are tight folds (Table 1).

Based on the dip of the axial plane, T1, T2, and T6 are upright folds; T3, T4, and T5 are steeply inclined folds, and T7 is moderately inclined fold. According to the hinge plunge of the fold, all of the folds in the Shekarab area are gently plunging except T1 and T3 folds (Figure 6).

The geometric characteristics of the folded layers in the Shekarab area (limbs of T1 to T7) are plotted on the Wulff net (Figure 7). Using these characteristics, the positions of the σ_1 , σ_2 , and σ_3 were calculated by the stereonet program (see

Figure 7; Table 2). The method applied in the program is based on the axial planes and hinge lines of the folds. In flexural slip folds, the line perpendicular to the axial plane is a position of the compression (σ_1) that created the folds. Moreover, the σ_2 in a fold is equal to the position of the fold axis. Considering that the stress axes have a 90-degree distance from each other, the position of the σ_3 can be easily identified on the Wulff net (Davis and Reynolds, 1996).

The Shekarab folds, particularly T1 to T5, included the indicators of the slips between the folded layers. Tuff-limestone and sandstone rock units are the most essential lithological units that preserved the interlayer sliding. Many strike-slip fault planes parallel to layering have been created

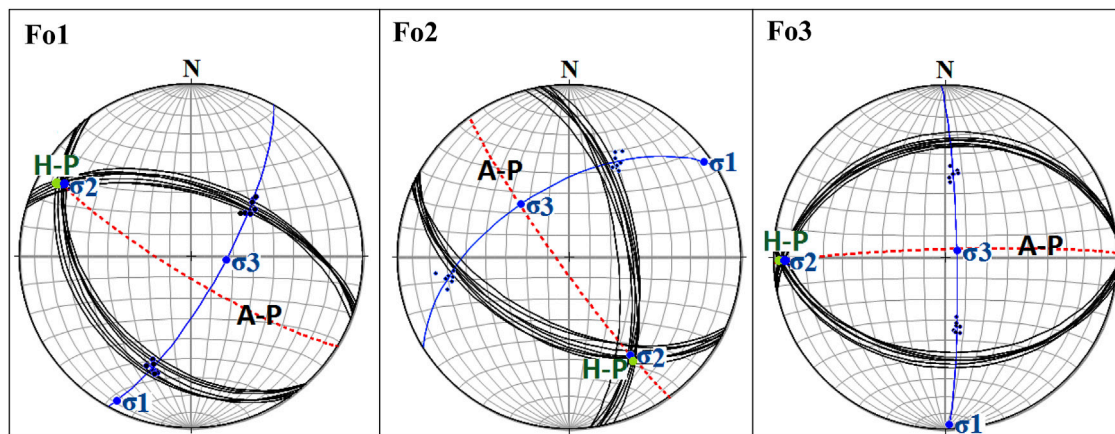


FIGURE 12
Stereogram, contour diagram, and principal stress axes (σ_1 , σ_2 , σ_3) of the Fo1, Fo2, and Fo3 folds in the Arc area. A-P= Axial plane; H-P= Hinge point.

within T1 to T5 folds due to their flexural-slip mechanism (Figure 8).

4.2 Structural style of the arc area

The Khouf anticlinal core, known as the Arc area, includes various geological structures such as parasitic folds, small-scale active folds with various axial-trace directions, and several fault planes with different mechanisms. Some faults, particularly strike-slip faults, cut the folded geological layers (Figure 9). The rock units' right-lateral and left-lateral offsets are clearly seen along them.

We obtained two geological profiles with NNE-SSW directions (A-A', B-B'; Figure 9) on the Arc folds (Fo1-Fo2, and Fo3; Figure 9) by Digital Elevation Model (DEM), detailed geological map, and fieldwork data (Figure 10). We used the profiles to determine the geometry of the folds and the amount of shortening by their restored profiles where there is Khouf anticlinal core.

Across the considered profiles, the geometric characteristics of the folds and their wavelengths were carefully measured to prevent overestimating the structural reliefs to estimate the amount of shortening. Evaluating the structural reliefs in the area indicated thickness variations in the folded rock units in different parts of the profiles. These profiles included high-relief synclines and eroded anticlines.

Along the A-A' profile, the structural elevation decreases from the NE toward the SW. The average structural height for this profile is ~1700 m, and the highest relief is related to the Fo1 fold (Figure 10A). Along the A-A' profile, the post-Cretaceous and Eocene rock units are exposed on the ground surface, and rarely are there Quaternary sediments. Along the profile, the post-Cretaceous flysch units are more folded (Figures 10, 11). The B-B' profile includes a big syncline with the highest relief (2,150 m) in its middle part (Figure 10B). Most deformations are related to the folded post-Cretaceous flysch units in the middle part of the profile.

The A-A' profile with a length of ~4.8 km and its restored profile with a length of ~5.5 km indicated ~0.7 km (~14%) shortening (Figure 10A). The B-B' profile, with ~8.5 km length after restoration, its length was ~9.3 km. Therefore, the shortening along this profile was ~0.85 km (10%) (Figure 10B).

Like the structural analysis of the Shekarab folds, we conducted Arc folds geometry classification (e.g., aspect ratio, interlimb angle, fold bluntness, Fourier coefficients, fold shapes, tightness, and amplitude numbers definition) using the satellite images and geological profiles, which were obtained by DEM, detailed geological map, and fieldwork, with the equations related to the fold geometry (see the "Data and Methodology" section).

The attitudes of the northeastern and southwestern limbs of the Fo1 fold measured ~N40W°, 30°SW and ~N60W°, 60°NE, respectively. In Ramsay's (1967) dip isogon categories, this syncline is located between classes 1B and 1C. The attitudes of the northeastern and southwestern limbs of the Fo2 fold are ~N60W°, 50°SW, and ~N20W°, 60°NE, respectively. Our measurements on the limb layers showed that the Fo2 syncline, like the Fo1 syncline (both related to the A-A' profile), is located between classes 1B and 1C in Ramsay's dip isogon categories (Ramsay J. G., 1967; Ramsay J. G., 1967). The Fo3 fold, which is related to the B-B' profile, includes class 1A. The attitudes of its northern and southern limbs are ~N90W°, 40°S, and ~N80E°, 35°N, respectively.

Based on the fold style and fold shape, the Fo1 and Fo2 folds are both broad and between semi-ellipses and parabolas (Table 3; Figure 6). According to the fold tightness classifications, the Fo1 and Fo2 folds are open and closed, respectively (Table 3).

In classifications of the fold style, fold tightness, and fold shape, the Fo3 is a wide, gentle, and semi-ellipsoidal fold (Table 3; Figure 6).

In the Fleuty classification (Fleuty, 1964) based on the dip of the axial surface and plunge of the hinge line, the Fo1, Fo2, and Fo3 folds are located in the upright inclined gently plunging, upright inclined moderately plunging, and upright inclined horizontal plunging class, respectively (Table 4; Figure 6).

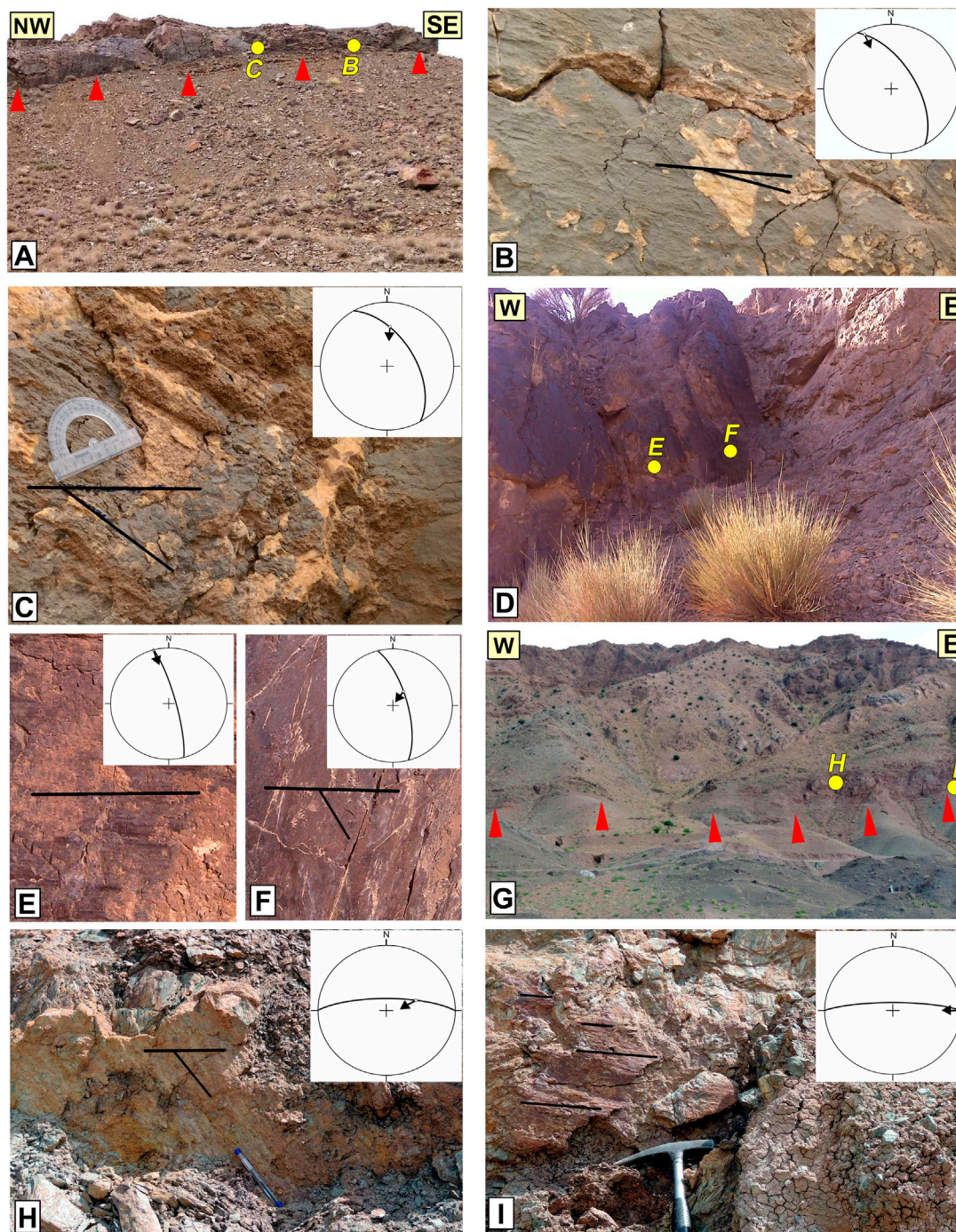


FIGURE 13

Field evidence of three fault zones (as case studies) shows interlayer slips in the different parts of the Khouf folded platform. See the locations in [Figure 2B](#). (A) Fault slip planes in the left limb of the Khouf anticline with attitudes of $N30^{\circ}W, 60^{\circ}NE$ and $N30^{\circ}W, 55^{\circ}NE$. (B, C) Close-up view of the fault planes with slickenlines of $335^{\circ}/8^{\circ}$ and $004^{\circ}/38^{\circ}$. (D) Fault slip planes in the right limb of the Khouf syncline with attitudes of $N15^{\circ}W, 80^{\circ}NE$ and $N15^{\circ}W, 70^{\circ}NE$. (E, F) Close-up view of the fault planes with slickenlines of $345^{\circ}/00^{\circ}$ and $036^{\circ}/65^{\circ}$. (G) Fault slip planes in the common limbs of the Khouf anticline and syncline with attitudes of $N90^{\circ}E, 75^{\circ}N$ and $N90^{\circ}E, 80^{\circ}N$. (H, I) Close-up view of the fault planes with slickenlines of $070^{\circ}/52^{\circ}$ and $090^{\circ}/00^{\circ}$.

We plotted the geometric characteristics of the folded layers in the Arc area (limbs of Fo1, Fo2, and Fo3) on the Wulff net ([Figure 12](#)). On the basis of their characteristics, the positions of the σ_1 , σ_2 , and σ_3 were measured using the stereonet program (see [Figure 12](#); [Table 4](#)).

4.3 Parasitic folds and layer-parallel slip planes in the Khouf folded platform

In the Khouf folded platform, the movement planes at the boundaries of the packets of the rock units are known as the essential

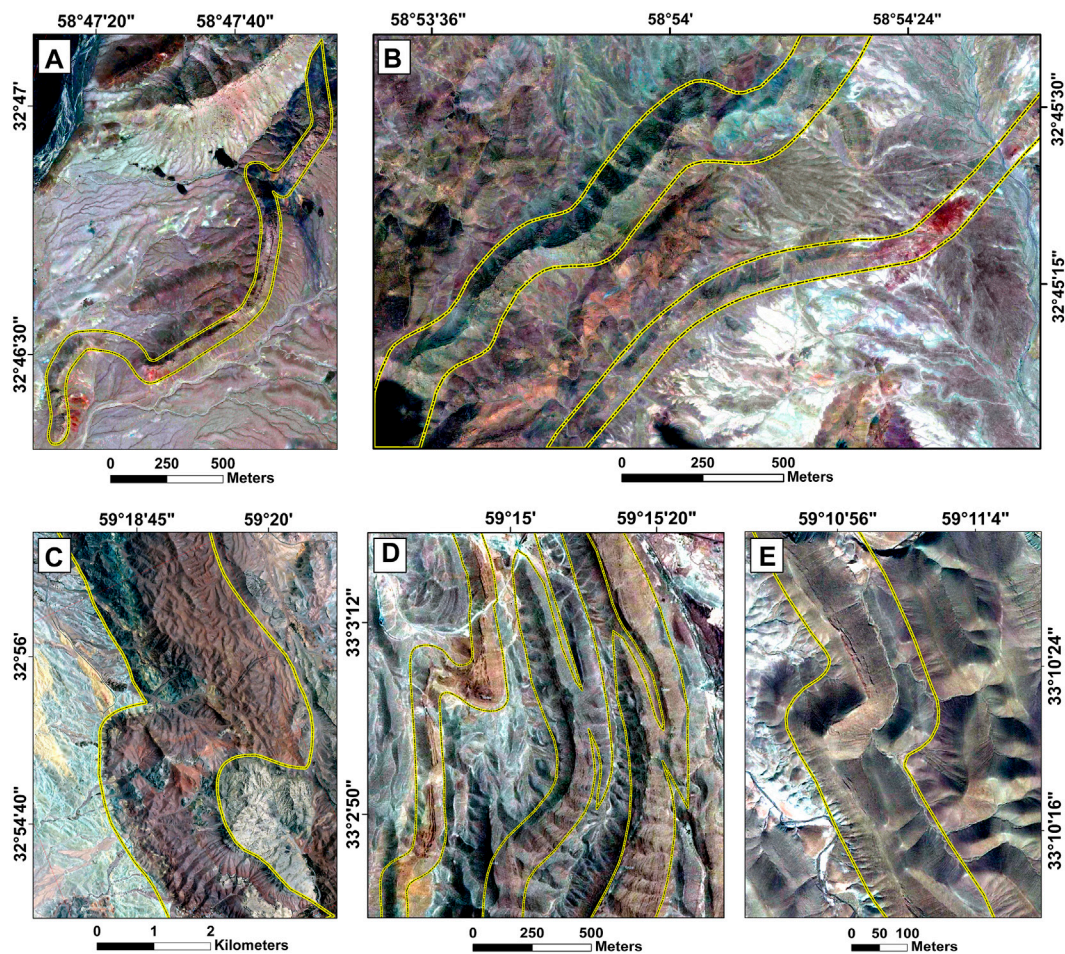


FIGURE 14

Examples of the Z-folds within the Khouf folded platform. (A, B) Z-folds on the left limb of the Khouf anticline. (C–E) Z-folds on the right limb of the Khouf syncline. See the locations in [Figure 2](#).

faults which have created the small-scale geological structures (e.g., folds, parasitic folds, duplexes) ([Rashidi et al., 2022a](#)). These faults (e.g., see [Figure 13](#)) include planes with various movement senses, such as right-lateral strike-slip, left-lateral strike-slip, reverse, and their composite components.

We carefully determined the layers' parallel slip planes on the limbs and cores of the Khouf anticline and syncline (see [Figures 2, 13](#)). Fault slickenlines indicated that strike-slip planes (with ~N-S strikes) in the left limb of the anticline and right limb of the syncline have right-lateral strike-slip mechanism, and the strike-slip planes (with ~E-W strikes) on the common limbs of the anticline and syncline have left-lateral strike-slip mechanism ([Figures 2, 13](#)).

In [Figure 13](#), we present the field evidence of three faults (as case studies) that show interlayer slips. Each fault includes several planes with a different mechanism, which emphasizes the slip partitioning on the folded platform.

On the left limb of the Khouf anticline, the fault zones, which include two principal planes with attitudes of N30°W, 60°NE, and N30°W, 55°NE are located among the Cretaceous flysch layers ([Figure 13A](#)). These fault planes with slickenlines of 335°/8° and

004°/38° indicated a left-lateral strike-slip mechanism with a reverse component and a reverse mechanism with a left-lateral element, respectively ([Figures 13B, C](#)). On the right limb of the Khouf syncline, planes of the fault with attitudes of N15°W, 80°NE; N15°W, 70°NE showed a right-lateral strike-slip mechanism and reverse mechanism with right-lateral strike-slip component ([Figure 13D](#)). Their slickenlines are 345°/00° and 036°/65°, respectively ([Figures 13E, F](#)).

The Shekarab fault is a case study of the interlayer slip on the common limb of the Khouf anticline and syncline. It includes two principal parallel planes in most of its length that follow the contact of the Cretaceous ophiolitic mélanges to the north and Eocene basaltic andesite to the south ([Figures 2, 13G](#)) ([Eftekharnajad et al., 1978](#)). One of the fault planes with attitudes of N90°E, 75°N, and slickenlines of 070°/52° has a reverse mechanism with a left-lateral strike-slip component ([Figure 13H](#)). Another plane with attitudes of N90°E, 80N, and slickenlines of 090°/00° indicated left-lateral strike-slip mechanism ([Figure 13I](#)).

In the following, we present some geological structures (e.g., parasitic folds) among the fault planes, which show interlayer slips (the layer-parallel slip planes) in the limbs and cores of the Khouf

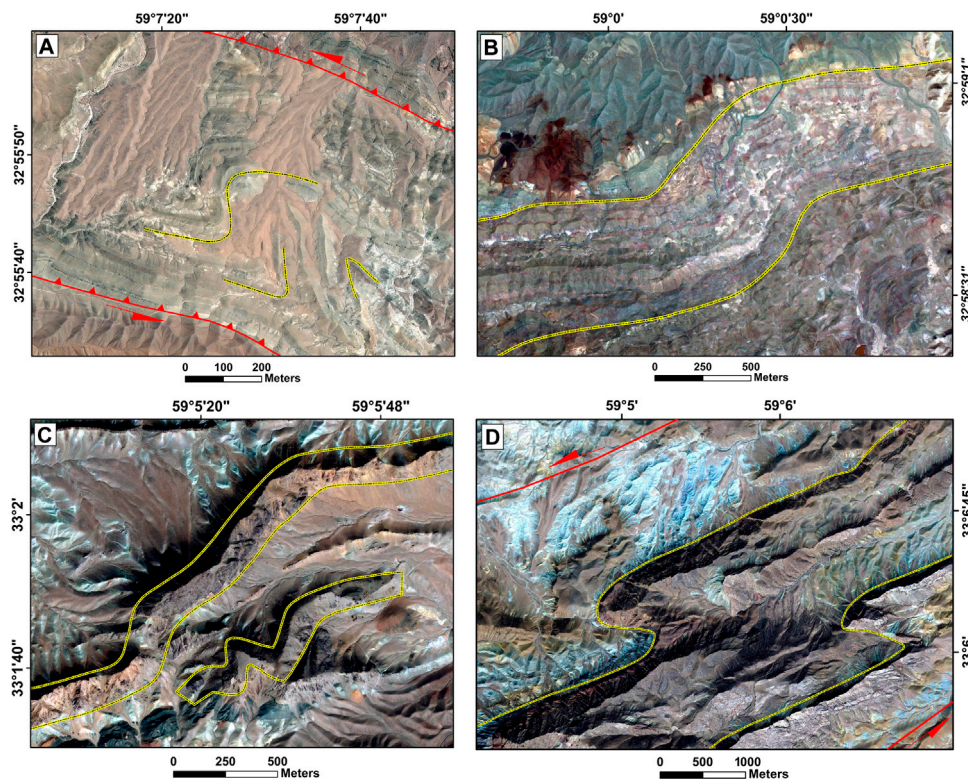


FIGURE 15

Four examples of the S-folds (A–D) within the common limbs of the Khouf anticline and syncline. The locations of these folds are indicated in Figure 2.

folded platform which confirms a sense of slips on the different parts of the platform.

Large-scale folds (e.g., Khouf folded platform) usually include smaller-scale folds in its cores and limbs. Some smaller-scale folds are commonly called parasitic folds or passive flow folding (de Sitter, 1958; Geoff Tanner, 1989). These folds with Z, S, M, and W shapes are created during the flexure of rock layers, where slips happen between the layers (de Sitter, 1958). Determining the geometric position of these folds, particularly Z- and S-folds, are extremely useful for structural analysis of the large-scale folds affected by buckling orogeny phases. Generally, Z- and S-folds are located in the limbs of anticlines and synclines, and M- and W-folds are found in the cores of synclines and anticlines (Ramsay and Huber, 1987).

We used the Bing map aerial imagery to determine parasitic folds in different parts of the large-scale Khouf folded platform (Figures 14, 15, 16). The parasitic folds in the Khouf folded platform due to the various buckling phases of the East Iran orogenic and progressive deformation have different wavelengths, amplitudes, and sizes so that some of them can emphasize different generations of folding in various stages of deformations (e.g., Figures 14B, D, 15C). Our structural findings of the platform present the Z-folds on the left limb of the anticline (Figures 14A, B) and the right limb of the syncline (Figures 14C–E).

The common limbs of the Khouf anticline and syncline included various geological structures, particularly duplexes and parasitic folds. All parasitic folds in the common limbs are S-folds

that were formed by interlayer slips. Figure 15 includes examples of the S-folds in different parts of the common limbs. As a result of the progressive deformation within layers' parallel slip planes, the S-folds axes have rotated and usually displace the rock units along their axes. Therefore, the duplexes structure has been formed in the common limbs [see Rashidi et al. (2021) for details].

The amplitude of M and W parasitic folds during progressive deformation grows continuously. It is noteworthy, however, that if the more prominent fold has experienced several generations of folding and it is an asymmetric fold, then the amplitude of the parasitic folds (M- and W-folds) in some parts of the folds cores may not grow much. In Figure 16, we present two examples of the M-folds and W-folds on the cores of the Khouf anticline and syncline.

5 Discussion

Rheological properties of the layers are influential parameters in determining the folding process and shape of folds (Hudleston and Treagus, 2010; Schmalholz and Mancktelow, 2016). Various studies have been conducted on this topic. Ramsay (Ramsay J. G., 1967; Ramsay J. G., 1967) presented an early overview of analogue materials with measurable viscosities (gelatin and plasticine). Some researchers (Abbassi and Mancktelow, 1992; Mancktelow and Abbassi, 1992; Casey and Butler, 2004; Reber et al., 2010)

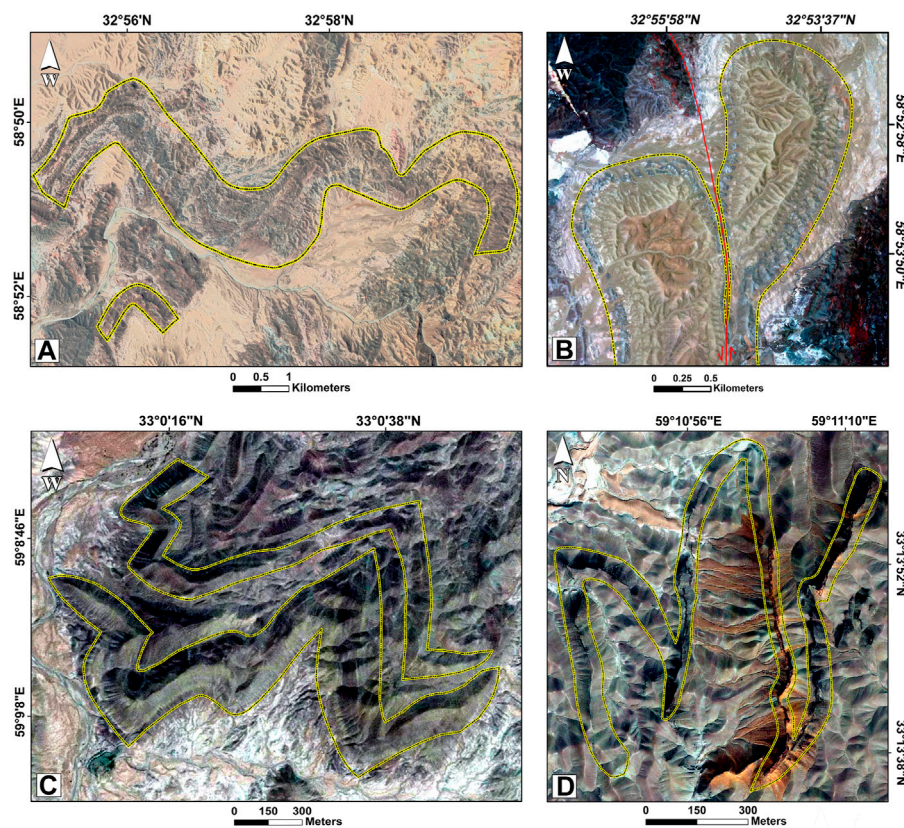


FIGURE 16

Examples of the M- and W-folds within the Khouf folded platform. (A, B) M-folds on the Khouf anticline core. (C, D) W-folds on the Khouf syncline core. See the locations in Figure 2.

applied numerical methods to understand the buckle folding processes. A multilayer may have a large, moderate, or small competence contrast among the different layers. The competence contrast between layers influences the shape of folds. As for single embedded layers, the thicker and stiffer multilayers tend to produce larger wavelength rounded folds (McClay, 2012). Hence, buckle-folded multilayers show a wider range of fold shapes than buckle-folded single layers. For example, multilayer, both in nature and in model experiments, may show round-hinged folds, chevron folds, and conjugate folds (McClay, 2012). However, the buckle folds in our study area have different shapes (see Tables 1, 2, 3, 4).

The Abiz, Sedeh, Khouf, Nowzad, Birjand, Hashtooan, and Qaryan are known as the most important northern splays of the N-S strike-slip systems (e.g., West Neh and East Neh) within the East Iran orogenic (Figure 1C). The rheology of the rock units that make up the splays determines the deformation type, which can be brittle, ductile, brittle-ductile, or ductile-brittle (Ramsay and Huber, 1987). Instead of faulting, rock units may fold or bend in a ductile manner. Sometimes rock units that we typically consider brittle can fold due to the low rate of stress (Zang and Stephansson, 2010). However, brittle rock units tend to fracture when under enough stress. One of the splays of eastern Iran with ductile behavior is the Khouf splay (Figure 1C). The most important structures of this splay are folds (Tirrul et al., 1983; Bagheri and Damani Gol, 2020).

In orogenic belts with long deformation history (e.g., East Iran orogen), the general patterns of the deformations (e.g., folds) are related to buckling phases of orogenic belts during various geological times. Here, we used the drastic temporal changes in the stress regimes of East Iran orogenic during the post-late Cretaceous, which have been published by some researchers (Jentzer et al., 2017; Ezati et al., 2022b) (Figure 17). Directions of the maximum stress (σ_1) in the late-Cretaceous-late Paleocene, Eocene-Oligocene, Miocene, late Miocene-late Pliocene, and Quaternary have been obtained as N290° (Ezati et al., 2022b), N035° (Ezati et al., 2022b), N090° (Jentzer et al., 2017), N060° (Jentzer et al., 2017), and N045° (Ezati et al., 2022b), respectively (Figure 17). Therefore, by changing the stress regime, the characteristics of folds and faults related to the splays (e.g., geometry, mechanism, and strain rates) could have changed several times.

Lateral transport of the fold axes commonly occurs during progressive deformation in buckling phases of orogenic belts (Alsop, 1992; Carreras and Druguet, 2019). Figures 3, 9, 18, presenting the folds with different axial-trace directions, emphasize the effect of the progressive deformations and changes of post-late Cretaceous buckling phases on the fold geometries in eastern Iran. Therefore, in the East Iran orogenic, the series of secondary folds had been superimposed on previous folds.

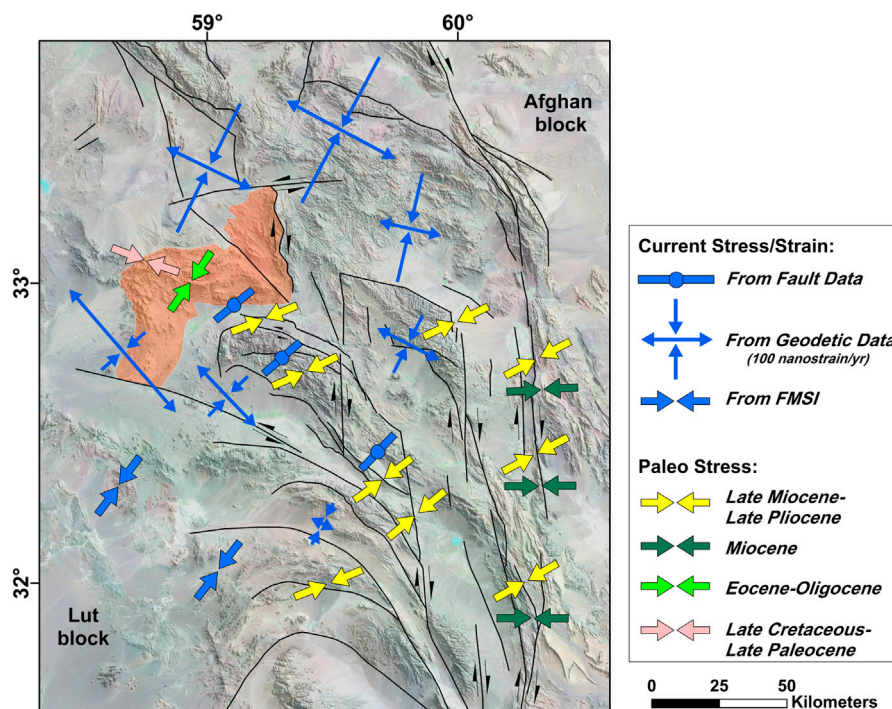


FIGURE 17

The post-late Cretaceous buckling phases with geodetic strain map of the northern domain of the East Iran orogenic. The current-day strain and stress directions are as a result of the inversions of geodetic and fault slip data, respectively, adapted from (Rashidi et al., 2022b). The focal mechanism stress inversions (FMSI) are based on Sheikholeslami et al. (2021) and Rashidi et al. (2022b). The presented paleo-stress data are from Jentzer et al. (2017) and Ezati et al. (2022b).

In the Khouf folded platform, continued compression caused the buckled layer to buckle again. Refoldings, due to the changing stress directions, have formed complex structures. Our structural investigations of the post-late Cretaceous folded rock sequences in the study area show at least two important generations of the folding with the E-W and NE-SW axes (Figure 2). These folds can be seen in different parts of the Khouf folded platform (Figure 2).

The folded Eocene rock units in the northern and southern domains of the platform have dip directions of the south and north, respectively (see Figure 2). Strongly folded Cretaceous flysch are outcropped within the platform and between the folded Eocene rock units (Figure 2A). Our geological and structural maps (Figure 2) indicate consecutive anticlines and synclines in an NNW-SSE profile (Figure 19A) where their upper parts have been eroded. The erosion has caused the rock units older than Eocene (e.g., Cretaceous rock units) to be exposed on the ground surface.

In a NE-SW profile, the Khouf folded platform includes the plunging anticline and syncline (Khouf anticline and syncline), which are visible on the ground surface (Figure 2). Therefore, buckling folds with different mechanisms and geometry has been created on the platform.

5.1 Folds flexural-slip mechanism

In the orogenic belts, in response to the lateral shortening, flexural folds are created as a result of one layer slipping over another during

the increases of limb dip (known as flexural-slip mechanism) and also using the simple dominant shear within the rock units (known as flexural-flow mechanism), or even by combinations of these two processes (Donath and Parker, 1964). A flexural slip mechanism can be formed in the chevron folding (Ramsay, 1974). This mechanism can be the primary process until the folds “lock up” within inter-limb angles of $\sim 60^\circ$ (Kuenen and Sitter, 1938; de Sitter, 1958). Flexing the beds in this mechanism can create flexural-flow folding within packets of the rock units (Kölbel, 1940; Hoeppeck, 1953).

There are some studies related to the flexural mechanisms, such as the role of flexural slip during the development of chevron folds (Wu et al., 2019); lithospheric folding by a flexural slip in subduction zones (Romeo and Álvarez-Gómez, 2018); the mechanisms of flexural flow folding of competent single-layers (Torremans et al., 2014), and non-cylindrical flexural-slip folds (Dubey, 1997). In this study, we provided detailed evidence to analyze the folding mechanisms of the large-scale Khouf folded platform and its smaller-scale folds to figure out the tectonic evolution models of an old ductile splay (Khouf folded platform) in the East Iran orogenic. Our structural analysis of the field evidence (e.g., interlayer slips; Figure 8), fold geometry classifications (see Tables 1, 2, 3), and structural shortening demonstrated that most of the folds within the Khouf folded platform have a flexural-slip mechanism. In addition, our field evidence of the large-scale Khouf anticline and syncline (see Figure 13) indicated interlayer slips resulted from the flexural-slip mechanism.

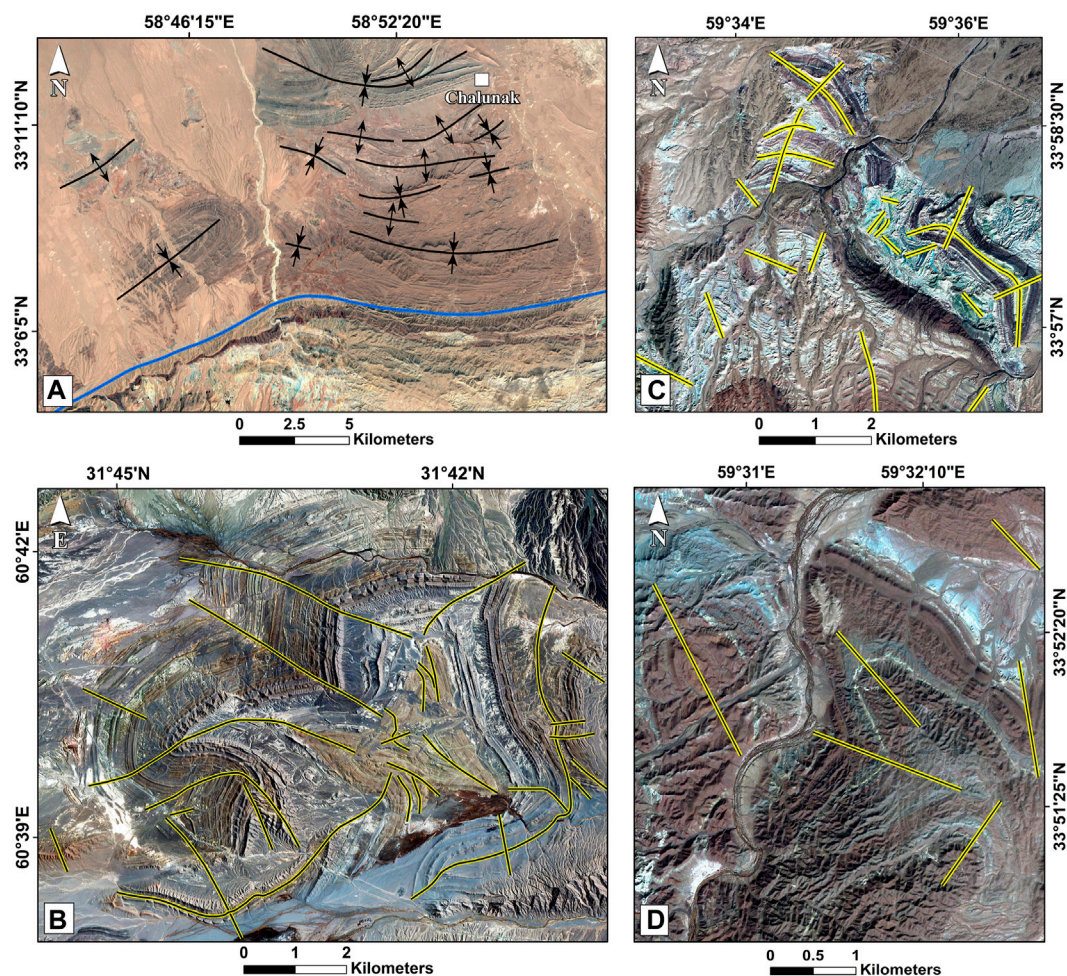


FIGURE 18

Examples of the folds with different axial-trace directions and refoldings with complex structures resulted of the various buckling phases of the East Iran orogenic. (A) The folds with different axial-trace directions in the northern domain of the Khouf folded platform. (B) Refoldings with different axial-trace directions in the southeastern domain of the northern part of the East Iran orogenic. (C, D) Refoldings and folds with different axial-trace directions in the northern domain of the East Iran orogenic. See the locations in [Figure 1C](#).

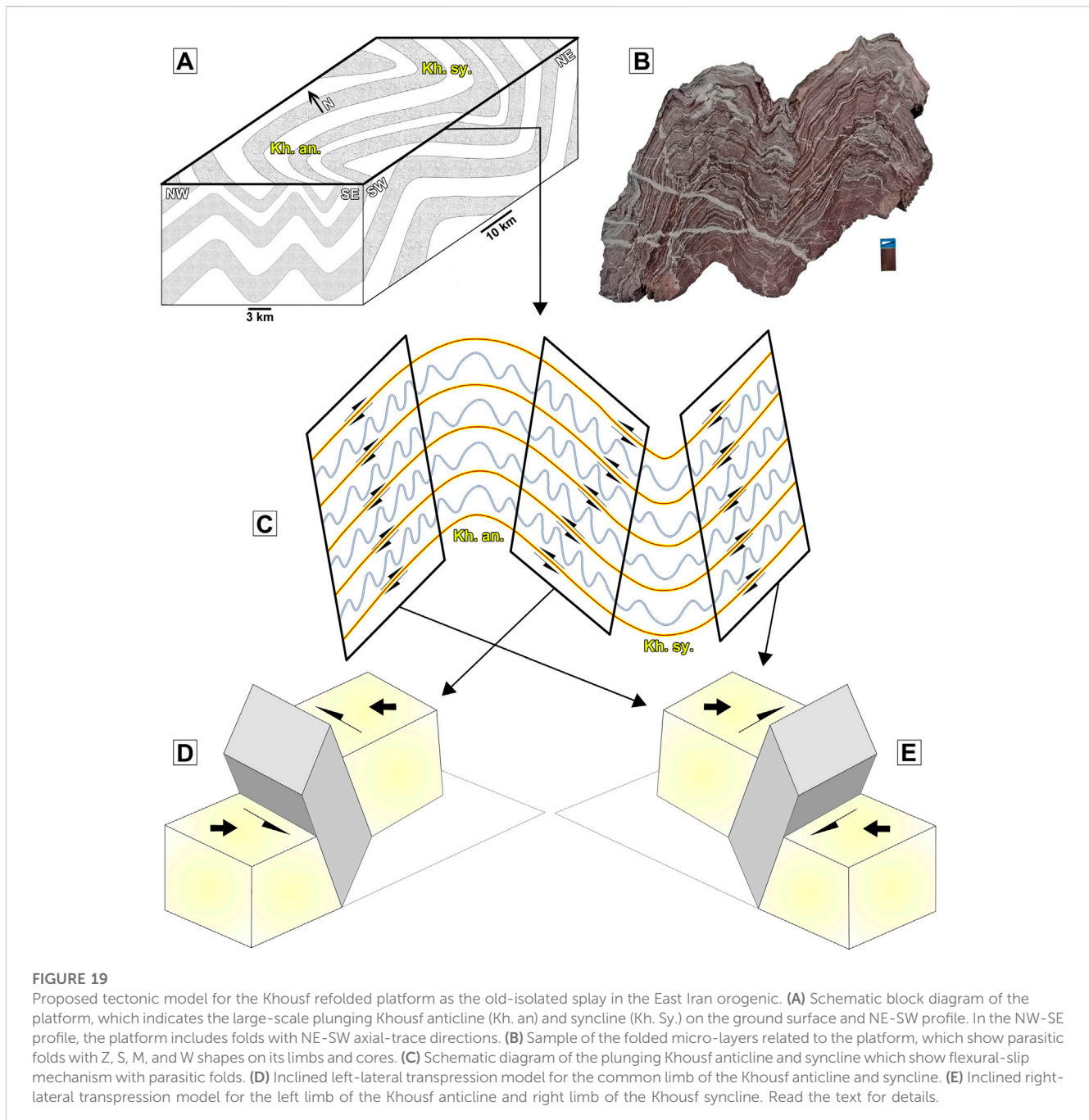
5.2 Slip partitioning and transpression deformation

In the Khouf folded platform, fault planes parallel to the beds have various mechanisms such as strike-slip, reverse, and a combination of both (see [Figure 13](#)). These movement planes have generated various geological structures (e.g., parasitic folds, folds with and without plunging, and duplexes) in different parts of the platform. Strike-slip planes on the left limb of the Khouf anticline and the right limb of the Khouf syncline have right-lateral movements, while strike-slip planes on the common limbs of the anticline and syncline have left-lateral movements. One of the consequences of these movements has been Z-folds and S-folds within the packets of the rock units where there were right-lateral and left-lateral movements, respectively (see [Section 4.3](#) and [Figure 19B](#)). In [Figure 19C](#), we presented the parasitic folds on the horizontal surface within the limbs of the Khouf folded platform. Another consequence of the strike-slip movements was the generation of the shear duplex structure

within the packets of the Eocene rock units on the common limb of the Khouf anticline and syncline, which has been investigated in detail by [Rashidi et al. \(2022c\)](#).

Other movement planes parallel to the platform beds have a reverse mechanism and reverse mechanism with a strike-slip component. These fault planes have generated some active folds and caused an uplift of the Khouf platform limbs. However, our structural evidence indicates a combination of simple shear with pure shear on the platform limbs. This study emphasizes the slip partitioning and transpression deformation in forming the structural features related to the Khouf folded platform with flexural-slip mechanism.

Transpression zones resulting from oblique convergence of the tectonic plates include a combination of shortening (or extension) and shear movements along the shear zones ([Harland, 1971](#); [Dewey et al., 1998](#)). Several models have been applied to show transpression in the different areas of the ground surface ([Sanderson and Marchini, 1984](#); [Mukherjee and Koyi, 2010](#)). A common feature of transpressional is the inclined transpression model, which



includes the simultaneous action of contraction and oblique-slip shear (Jones et al., 2004). Oblique-slip shear can be separated into a strike-slip and a dip-slip component (Mukherjee and Koyi, 2010). In the inclined transpression zone, strain partitioning is in the form of folds with the different plunging of hinge lines (0° – 90°) and faults with reverse, normal, and strike-slip mechanisms (Jones et al., 2004). Generally, the geological structures of the study area follow the strain triangle in the inclined transpression model so that its contractional components usually are found in the folds that are steeply plunging to moderately plunging, and folds that are upright horizontal to moderately inclined. NW-SE dominated folds without plunging, and NW-SE thrust faults emphasize the dip-slip

component. Left-lateral and right-lateral strike-slip faults with their shear fractures indicates strike-slip component of the strain partitioning in the inclined transpression zone.

Transpression deformation zones have been identified in the southern Uplands of Scotland (Tavarnelli et al., 2004); the central Myanmar basin (Khin et al., 2021); the central Iran microcontinent of SE Iran (Ebrahimi et al., 2021); the Zagros of Iran (Rahnamarad et al., 2008; Ghanbarian et al., 2021); and Alborz in northern Iran (Nabavi et al., 2017). According to our structural evidence of the Khouf folded platform, our proposed model is inclined transpression for each limb of the platform. For the common limb of the Khouf anticline and syncline, we suggest the

inclined left-lateral transpression model (Figure 19D), and for the left limb of the Khouf anticline and the right limb of the Khouf syncline, we suggest the inclined right-lateral transpression model (Figure 19E). Therefore, the tectonic evolution of the geological structures in this part of East Iran orogenic follows a large-scale refolded flexural-slip fold (Khouf folded platform), where its limbs indicate inclined transpression deformation zones.

6 Conclusion

The findings of this study provide a new and detailed tectonic evolution model for the ductile old splay in the East Iran orogen. The Khouf refolded platform, which is a large-scale refolded flexural-slip fold, has been identified as a key feature in the region. The platform includes a large-scale plunging anticline and syncline that, in their limbs and cores, contain smaller-scale geological structures such as active folds, parasitic folds, and duplexes. These structures have been analyzed using various methods such as geometric-kinematic relationships, interlayer slipping, and fold geometry classifications.

The novelty of this study lies in the detailed structural analysis of the Khouf refolded platform and its smaller-scale structural features. Our study has identified two main generations of folding with the ~ENE-WSW and NW-SE axes, caused by Arabia and Indian-Eurasia convergence. The Khouf refolded platform has undergone a flexural-slip mechanism, which has given rise to various structural features, including parasitic folds with M, W, Z, and S shapes. The study also identifies the inclined transpression deformation zones in the limbs of the platform, and the inclined right-lateral and left-lateral transpression models in the limbs and cores of the Khouf anticline and syncline.

Our field data indicated that the Khouf refolded platform includes large-scale plunging anticlines and synclines where, in their limbs and cores, some smaller-scale geological structures (e.g., active folds, parasitic folds (passive flow folds), duplexes) had been formed. We obtained the structural style of the Shekarab folds at the common limbs of the anticline and syncline, and the Arc folds at the core of the anticline.

In the Shekarab area, the folds (T1 to T7) have different axial-trace directions. The amount of shortening of the T1 to T5 folds in the NE-SW direction was calculated at ~33%. Shortening values of the T6 and T7 folds on the N-S and NW-SE directions were calculated at ~65% and ~68%, respectively. Based on the tightness classification, the T1 and T2 are close, T3 and T4 are open, T5 is gentle, and T6 and T7 are tight folds. The T7 fold, which shows the maximum value of the shortening, is an overturned chevron syncline.

In the Arc area, the Fo1 and Fo2 folds have undergone ~14% shortening in the NE-SW direction, while the Fo3 fold has experienced ~10% shortening in the N-S direction. The Fo1, Fo2, and Fo3 folds are classified as open, closed, and gentle, respectively. The Fourier analysis of fold shapes indicates that most of these folds are semi-ellipses and have high wavelengths.

The Khouf refolded platform is characterized by a series of secondary folds (Khouf plunging anticline and syncline) with NW-SE axes directions superimposed on previous folds with the ~ENE-WSW axes direction. In the N-S profile, we determined

consecutive anticlines and synclines (as the first-generation folds) on the platform. Our structural analysis of the field data has revealed that the Khouf refolded platform and the active folds within its limbs and cores have a flexural-slip mechanism. To determine the tectonic evolution model of the Khouf refolded platform, we obtained the geometric-kinematic relationship of the platform with its smaller-scale structural features. Flexing of the beds has given rise to flexural flow within some beds, leading to the formation of parasitic folds with M, W, Z, and S shapes in the cores and limbs of the Khouf anticline and syncline. These structures are the result of the right-lateral shear sense on the left limb of the anticline and right limb of the syncline, and the left-lateral shear sense on the common limb of the anticline and syncline.

Based on our analysis of the basic folding mechanisms, we present a new tectonic evolution model for the ductile old splay in the East Iran orogen, which follows a large-scale refolded flexural-slip fold (Khouf refolded platform) with inclined transpression deformation zones in its limbs. Therefore, the left limb of the Khouf anticline and the right limb of the Khouf syncline follow the inclined right-lateral transpression model, while the common limb of the Khouf anticline and syncline follows the inclined left-lateral transpression model. This new tectonic evolution model is of great importance in the understanding of the geological structures in the East Iran orogenic. The detailed structural analysis of the Khouf refolded platform and its smaller-scale structural features can provide a new framework for future studies on similar structures in other regions and can contribute to the development of a broader understanding of large-scale geological structures and their formation mechanisms.

Data availability statement

The raw data supporting the conclusion of this article will be made available by the authors, without undue reservation.

Author contributions

AR, formal analysis, methodology, fieldwork, investigation, writing the first draft of the manuscript, supervision; SS, conceptualization and design of the study, review, and editing; MN and RD, resources; methodology, validation, visualization, writing, review, and editing; ME, EG, and SM, visualization, review, and editing. All authors have read and agreed to the published version of the manuscript. All authors contributed to the research and preparation of the manuscript and approved the submitted version.

Acknowledgments

This study was mainly supported by the Shahid Bahonar University of Kerman, Kerman, Iran; International Institute of Earthquake Engineering and Seismology, Tehran, Iran;

University of Birjand, Birjand, Iran; Utrecht University, Utrecht, Netherlands.

Conflict of interest

The authors declare that the research was conducted in the absence of any commercial or financial relationships that could be construed as a potential conflict of interest.

References

- Abbassi, M. R., and Mancktelow, N. S. (1992). Single layer buckle folding in non-linear materials-I. Experimental study of fold development from an isolated initial perturbation. *J. Struct. Geol.* 14. doi:10.1016/0191-8141(92)90147-O
- Alsop, G. I. (1992). Progressive deformation and the rotation of contemporary fold axes in the Ballybofey Nappe, north-west Ireland. *Geol. J.* 27, 271–283. doi:10.1002/gj.3350270305
- Ambraseys, N. N., and Tchalenko, J. S. (1969). The dasht-e bayāz (Iran) earthquake of august 31, 1968: A field report. *Bull. Seismol. Soc. Am.* 59, 1751–1792. doi:10.1785/BSSA0590051751
- Bagheri, S., and Damani Gol, S. (2020). The eastern Iranian orocline. *Earth Sci. Rev.* 210, 103322. doi:10.1016/j.earscirev.2020.103322
- Behrmann, J., Drodzowski, G., Heinrichs, T., Huch, M., Meyer, W., and Oncken, O. (1991). Crustal-scale balanced cross sections through the variscan fold belt, Germany: The central EGT-segment. *Tectonophysics* 196, 1–21. doi:10.1016/0040-1951(91)90287-3
- Berberian, F., and Berberian, M. (1981). “Tectono-plutonic episodes in Iran,” in *Geodynamics series*. Editors H. K. Gupta, F. M. Delany, and D. C. Washington (American Geophysical Union), 5–32. Available at: <http://www.agu.org/books/gd/v003/GD003p0005/GD003p0005.shtml>.
- Berberian, M., Jackson, J. A., Qorashi, M., Khatib, M. M., Priestley, K., Talebian, M., et al. (1999). The 1997 may 10 Zirkuh (Qa' enat) earthquake (Mw 7.2): faulting along the Sistan suture zone of eastern Iran. *Geophys. J. Int.* 136, 671–694. doi:10.1046/j.1365-246x.1999.00762.x
- Berberian, M., and King, G. C. P. (1981). Towards a paleogeography and tectonic evolution of Iran. *Can. J. Earth Sci.* 18, 210–265. doi:10.1139/e81-019
- Camp, V. E., and Griffis, R. J. (1982). Character, Genesis and tectonic setting of igneous rocks in the Sistan suture zone, eastern Iran. *Lithos* 15, 221–239. doi:10.1016/0024-4937(82)90014-7
- Carreras, J., and Druguet, E. (2019). Complex fold patterns developed by progressive deformation. *J. Struct. Geol.* 125, 195–201. doi:10.1016/j.jsg.2018.07.015
- Casey, M., and Butler, R. W. H. (2004). Modelling approaches to understanding fold development: Implications for hydrocarbon reservoirs. *Mar. Pet. Geol.* 21, 933–946. doi:10.1016/j.marpetgeo.2004.01.010
- Cloos, H., and Martin, H. (1932). Der gang einer Falte. *Fortschr. Geol. Paleontol.* 11.
- Davis, G. H. (2014). Quasi-flexural folding of pseudo-bedding. *Geol. Soc. Am. Bull.* 126, 680–701. doi:10.1130/B30963.1
- Davis, G. H., and Reynolds, J. S. (1996). *Structural geology of rocks and regions*. New York: John Wiley & Sons.
- de Sitter, L. U. (1958). Boudins and parasitic folds in relation to cleavage and folding. *Geol. Mijnb.* 20, 272–286.
- Delvaux, D., Kervyn, F., Macheyeki, A. S., and Temu, E. B. (2012). Geodynamic significance of the TRM segment in the East African Rift (W-Tanzania): Active tectonics and paleostress in the Ufipa plateau and Rukwa basin. *J. Struct. Geol.* 37, 161–180. doi:10.1016/j.jsg.2012.01.008
- Delvaux, D., Moeys, R., Stapel, G., Petit, C., Levi, K., Miroshnichenko, A., et al. (1997). Paleostress reconstructions and geodynamics of the Baikal region, Central Asia, Part 2. Cenozoic rifting. *Cenozoic Rift. Tectonophysics* 282, 1–38. doi:10.1016/S0040-1951(97)00210-2
- Delvaux, D., and Sperner, B. (2003). Stress tensor inversion from fault kinematic indicators and focal mechanism data: the TENSOR program. *Geol. Soc. Lond. Spec. Publ.* 212, 75–100. doi:10.1144/gsl.sp.2003.212.01.06
- Derakhshani, R., and Farhoudi, G. (2005). Existence of the Oman Line in the Empty Quarter of Saudi Arabia and its continuation in the Red Sea. *J. Appl. Sci.* 5, 745–752. doi:10.3923/jas.2005.745.752
- Derakhshani, R., Zaresefat, M., Nikpeyman, V., GhasemiNejad, A., Shafieibafti, S., Rashidi, A., et al. (2023). Machine Learning-Based Assessment of Watershed Morphometry in Makran. *Land (Basel)* 12, 776. doi:10.3390/land12040776
- Dewey, J. F., Holdsworth, R. E., and Strachan, R. A. (1998). Transpression and transtension zones. *Geol. Soc. Lond. Spec. Publ.* 135, 1–14. doi:10.1144/GSL.SP.1998.135.01.01
- Donath, F. A., and Parker, R. B. (1964). Folds and Folding. *Geol. Soc. Am. Bull.* 75, 45. doi:10.1130/0016-7606(1964)75[45:FAF]2.0.CO;2
- Dubey, A. K. (1997). Simultaneous development of noncylindrical folds, frontal ramps, and transfer faults in a compressional regime: Experimental investigations of Himalayan Examples. *Tectonics* 16, 336–346. doi:10.1029/96TC02231
- Ebrahimi, Y., Shafieibafti, S., Derakhshani, R., and Esmaeili, S. (2021). Slip partitioning and inclined transpression in the Bazargan fold and thrust belt, Central Iran Microcontinent, Kerman area, SE Iran. *J. Struct. Geol.* 148, 104352. doi:10.1016/j.jsg.2021.104352
- Eftekharnajad, J., Ohanian, T., and Tatevosian, S. (1978). *Geological map of the Birjand quadrangle*.
- Eftekharnajad, J. (1980). Subdivision of Iran into different structural realms with relation to sedimentary basins. *Bull. Iran. Pet. Inst.* 82, 19–28.
- Espurt, N., Angrand, P., Teixell, A., Labaume, P., Ford, M., de Saint Blanquat, M., et al. (2019). Crustal-scale balanced cross-section and restorations of the Central Pyrenean belt (Nestes-Cinca transect): Highlighting the structural control of Variscan belt and Permian-Mesozoic rift systems on mountain building. *Tectonophysics* 764, 25–45. doi:10.1016/j.tecto.2019.04.026
- Ezati, M., Gholami, E., Mousavi, S. M., Rashidi, A., and Derakhshani, R. (2022a). Active Deformation Patterns in the Northern Birjand Mountains of the Sistan Suture Zone, Iran. *Appl. Sci.* 12, 6625. doi:10.3390/app12136625
- Ezati, M., Rashidi, A., Gholami, E., Mousavi, S. M., Nemati, M., Shafieibafti, S., et al. (2022b). Paleostress Analysis in the Northern Birjand, East of Iran: Insights from Inversion of Fault-Slip Data. *Minerals* 12, 1606. doi:10.3390/min12121606
- Federico, L., Crispini, L., Vigo, A., and Capponi, G. (2014). Unravelling polyphase brittle tectonics through multi-software fault-slip analysis: The case of the Voltri Unit, Western Alps (Italy). *J. Struct. Geol.* 68, 175–193. doi:10.1016/j.jsg.2014.09.011
- Fleuty, M. J. (1964). The description of folds. *Proc. Geologists' Assoc.* 75, 461–492. doi:10.1016/S0016-7878(64)80023-7
- Fossen, H. (2016). *Structural geology* 2nd ed. Cambridge University Press.
- Freund, R. (1970). Rotation of Strike Slip Faults in Sistan, Southeast Iran. *J. Geol.* 78, 188–200. doi:10.1086/627500
- Geoff Tanner, P. W. (1989). The flexural-slip mechanism. *J. Struct. Geol.* 11, 635–655. doi:10.1016/0191-8141(89)90001-1
- Ghanbarian, M. A., and Derakhshani, R. (2022a). Systematic variations in the deformation intensity in the Zagros Hinterland Fold-and-Thrust Belt, Iran. *Z. Dtsch. Ges. fur Geowiss.* 173, 193–210. doi:10.1127/zdgg/2021/0276
- Ghanbarian, M. A., and Derakhshani, R. (2022b). The folds and faults kinematic association in Zagros. *Sci. Rep.* 12, 8350. doi:10.1038/s41598-022-12337-8
- Ghanbarian, M. A., Yassaghi, A., and Derakhshani, R. (2021). Detecting a sinistral transpressional deformation belt in the Zagros. *Geosci. (Basel)* 11, 226. doi:10.3390/geosciences11060226
- Ghassemi, M. R. (1990). *Geology, stratigraphy, and structural geology of Chahardeh area, eastern Alborz*. University of Tehran, 109. MSc Thesis: in Persian.
- Ghosh, S. K., Mandal, N., Sengupta, S., Deb, S. K., and Khan, D. (1993). Superposed buckling in multilayers. *J. Struct. Geol.* 15, 95–111. doi:10.1016/0191-8141(93)90081-K
- Hansen, E. (1971). “The Concept of Strain Facies,” in *Strain facies*. doi:10.1007/978-3-642-65080-2_9
- Harland, W. B. (1971). Tectonic transpression in Caledonian Spitsbergen. *Geol. Mag.* 108, 27–41. doi:10.1017/S0016756800050937
- Hashemi, F., Derakhshani, R., Bafti, S. S., and Raofi, A. (2018). Morphometric dataset of the alluvial fans at the southern part of Nayband fault, Iran. *Data Brief.* 21, 1756–1763. doi:10.1016/j.dib.2018.11.017

Publisher's note

All claims expressed in this article are solely those of the authors and do not necessarily represent those of their affiliated organizations, or those of the publisher, the editors and the reviewers. Any product that may be evaluated in this article, or claim that may be made by its manufacturer, is not guaranteed or endorsed by the publisher.

- Hibbard, J., van der Pluijm, B., and Marshak, S. (2004). *Earth Structure: An introduction to structural geology and tectonics* Second. W. W. Norton & Company.
- Hoeppenek, R. (1953). Faltung und Klüftung im Nordteil des Rheinischen Schiefergebirges. *Geol. Rundsch.* 41, 128–144. doi:10.1007/BF01803495
- Hudleston, P. J., and Stephansson, O. (1973). Layer shortening and fold-shape development in the buckling of single layers. *Tectonophysics* 17, 299–321. doi:10.1016/0040-1951(73)90044-9
- Hudleston, P. J., and Treagus, S. H. (2010). Information from folds: A review. *J. Struct. Geol.* 32, 2042–2071. doi:10.1016/j.jsg.2010.08.011
- Jackson, J., and McKenzie, D. (1984). Active tectonics of the Alpine—Himalayan Belt between western Turkey and Pakistan. *Geophys. J. Int.* 77, 185–264. doi:10.1111/j.1365-246X.1984.tb01931.x
- Jentzer, M., Fournier, M., Agard, P., Omrani, J., Khatib, M. M., and Whitechurch, H. (2017). Neogene to Present paleostress field in Eastern Iran (Sistan belt) and implications for regional geodynamics. *Tectonics* 36, 321–339. doi:10.1002/2016TC004275
- Jones, R. R., Holdsworth, R. E., Clegg, P., McCaffrey, K., and Tavarnelli, E. (2004). Inclined transpression. *J. Struct. Geol.* 26, 1531–1548. doi:10.1016/j.jsg.2004.01.004
- Kamali, Z., Nazari, H., Rashidi, A., Heyhat, M. R., Khatib, M. M., and Derakhshani, R. (2023). Seismotectonics, Geomorphology and Paleoseismology of the Doroud Fault, a Source of Seismic Hazard in Zagros. *Appl. Sci.* 13, 3747. doi:10.3390/app13063747
- Khin, K., Moe, A., Myint, M., and Aung, K. P. (2021). Dextral transpressional shearing and strike-slip partitioning developments in the Central Myanmar Basin during the collision between the India Plate and West Myanmar Block. *J. Asian Earth Sci.* X 5, 100055. doi:10.1016/j.jaesx.2021.100055
- Kim, Y.-S., Peacock, D. C. P., and Sanderson, D. J. (2004). Fault damage zones. *J. Struct. Geol.* 26, 503–517. doi:10.1016/j.jsg.2003.08.002
- Kölbel, H. (1940). Über Verformung von Klüften bei der Schichtenfaltung am Beispiel des Salzgitterer Sattels. *Geol. Rundsch.* 31, 188–197. doi:10.1007/BF01808393
- Kuenen, Ph. H., and Sitter, L. U. (1938). Experimental investigation into the mechanism of folding. *Leidsche Geol. Meded.* 10, 217–239.
- Leith, C. K. (1923). *Structural geology*. Nabu Press.
- Mancktelow, N. S., and Abbassi, M. R. (1992). Single layer buckle folding in non-linear materials-II. Comparison between theory and experiment. *J. Struct. Geol.* 14, 105–120. doi:10.1016/0191-8141(92)90148-p
- McClay, K. R. (2012). *Thrust tectonics*. Springer Science & Business Media.
- Mehrabi, A., Pirasteh, S., Rashidi, A., Pourkhosravi, M., Derakhshani, R., Liu, G., et al. (2021). Incorporating Persistent Scatterer Interferometry and Radon Anomaly to Understand the Anar Fault Mechanism and Observing New Evidence of Intensified Activity. *Remote Sens. (Basel)* 13, 2072. doi:10.3390/rs13112072
- Mukherjee, S., and Koyi, H. A. (2010). Higher Himalayan Shear Zone, Sutlej section: structural geology and extrusion mechanism by various combinations of simple shear, pure shear and channel flow in shifting modes. *Int. J. Earth Sci.* 99, 1267–1303. doi:10.1007/s00531-009-0459-8
- Nabavi, S. T., Díaz-Azpiroz, M., and Talbot, C. J. (2017). Inclined transpression in the neka valley, eastern Alborz, Iran. *Int. J. earth Sci.* 106, 1815–1840. doi:10.1007/s00531-016-1388-y
- Nemati, M., and Derakhshani, R. (2021). Short-term seismicity patterns along the most active faults in Iran. *J. Iber. Geol.* 47, 441–459. doi:10.1007/s41513-020-00133-0
- Nowroozi, A., and Mohajer-Ashjai, A. (1980). *Faulting of kurizan and koli (Iran) earthquakes of november 1979*. Bull. B.R.G.M.
- Qiu, L., Kong, R., Yan, D. P., Mu, H. X., Sun, W., Sun, S., et al. (2022). Paleo-Pacific plate subduction on the eastern Asian margin: Insights from the Jurassic foreland system of the overriding plate. *Bull. Geol. Soc. Am.* 134, 2305–2320. doi:10.1130/B36118.1
- Qiu, L., Yan, D. P., Tang, S. L., Wang, Q., Yang, W. X., Tang, X., et al. (2016). Mesozoic geology of southwestern China: Indosinian foreland overthrusting and subsequent deformation. *J. Asian Earth Sci.* 122, 91–105. doi:10.1016/j.jseas.2016.03.006
- Rahnmarad, J., Derakhshani, R., Farhoudi, G., and Ghorbani, H. (2008). Basement Faults and Salt Plug Emplacement in the Arabian Platform in Southern Iran. *J. Appl. Sci.* 8, 3235–3241. doi:10.3923/jas.2008.3235.3241
- Ramsay, J. G. (1974). Development of Chevron Folds. *Geol. Soc. Am. Bull.* 85, 1741. doi:10.1130/0016-7606(1974)85<1741:DOCF>2.0.CO;2
- Ramsay, J. G. (1967b). *Folding and fracturing of rocks*. Mc Graw Hill Book Company, 568. Available at: <https://cir.nii.ac.jp/crid/1572824498936667264.bib?lang=en> (Accessed March 25, 2023).
- Ramsay, J. G. (1967a). *Folding and fracturing of rocks (international series in the Earth and planetary sciences)*. The Blackburn Press.
- Ramsay, J. G., and Huber, M. I. (1987). *The techniques of modern structural geology: Folds and fractures* 1st ed. Academic Press.
- Rashidi, A., Abbassi, M.-R., Nilfouroushan, F., Shafiei, S., Derakhshani, R., and Nemati, M. (2020). Morphotectonic and earthquake data analysis of interactional faults in Sabzevaran Area, SE Iran. *J. Struct. Geol.* 139, 104147. doi:10.1016/j.jsg.2020.104147
- Rashidi, A., and Derakhshani, R. (2022). Strain and Moment Rates from GPS and Seismological Data in Northern Iran: Implications for an Evaluation of Stress Trajectories and Probabilistic Fault Rupture Hazard. *Remote Sens. (Basel)* 14, 2219. doi:10.3390/rs14092219
- Rashidi, A. (2021). Geometric and kinematic characteristics of the Khazar and North Alborz Faults: Links to the structural evolution of the North Alborz-South Caspian boundary, Northern Iran. *J. Asian Earth Sci.* 213, 104755. doi:10.1016/j.jseas.2021.104755
- Rashidi, A., Khatib, M. M., and Derakhshani, R. (2022a). Structural Characteristics and Formation Mechanism of the Earth Fissures as a Geohazard in Birjand, Iran. *Appl. Sci.* 12, 4144. doi:10.3390/app12094144
- Rashidi, A., Kianimehr, H., Shafieibafti, S., Mehrabi, A., and Derakhshani, R. (2021). Active faults in the west of the Lut block (Central Iran). *Geophys. Res.* 22, 70–84. doi:10.21455/gr2021.3-5
- Rashidi, A., Kianimehr, H., Yamini-Fard, F., Tatar, M., and Zafarani, H. (2022b). Present Stress Map and Deformation Distribution in the NE Lut Block, Eastern Iran: Insights from Seismic and Geodetic Strain and Moment Rates. *Pure Appl. Geophys* 179, 1887–1917. doi:10.1007/s00024-022-03015-x
- Rashidi, A., Shahpasandzadeh, M., and Braitenberg, C. (2022c). Late Cenozoic to Present Kinematic of the North to Eastern Iran Orogen: Accommodating Opposite Sense of Fault Blocks Rotation. *Remote Sens. (Basel)* 14, 4048. doi:10.3390/rs14164048
- Reber, J. E., Schmalholz, S. M., and Burg, J. P. (2010). Stress orientation and fracturing during three-dimensional buckling: Numerical simulation and application to chocolate-tablet structures in folded turbidites, SW Portugal. *Tectonophysics* 493, 187–195. doi:10.1016/j.tecto.2010.07.016
- Romeo, I., and Álvarez-Gómez, J. A. (2018). Lithospheric folding by flexural slip in subduction zones as source for reverse fault intraslab earthquakes. *Sci. Rep.* 8, 1367. doi:10.1038/s41598-018-19682-7
- Sanderson, D. J., and Marchini, W. R. D. (1984). Transpression. *J. Struct. Geol.* 6, 449–458. doi:10.1016/0191-8141(84)90058-0
- Schmalholz, S. M., and Mancktelow, N. S. (2016). Folding and necking across the scales: a review of theoretical and experimental results and their applications. *Solid* 7, 1417–1465. doi:10.5194/se-7-1417-2016
- Sengoer, A. M. C. (1979). Mid-Mesozoic closure of Permo-Triassic Tethys and its implications. *Nature* 279, 590–593. doi:10.1038/279590a0
- Şengör, A. M. C., Altner, D., Cin, A., Ustaömer, T., and Hsü, K. J. (1988). Origin and assembly of the Tethyside orogenic collage at the expense of Gondwana Land. *Geol. Soc. Lond. Spec. Publ.* 37, 119–181. doi:10.1144/GSL.SP.1988.037.01.09
- Şengör, A. M. C. (1984). *The cimmeride orogenic system and the tectonics of Eurasia*. Special Paper of the Geological Society of America, 195. doi:10.1130/SPE195-p1
- Sheikholeslami, M. R., Mobayen, P., Javadi, H. R., and Ghassemi, M. R. (2021). Stress field and tectonic regime of Central Iran from inversion of the earthquake focal mechanisms. *Tectonophysics* 813, 228931. doi:10.1016/j.tecto.2021.228931
- Shiells, K. A. G. (1963). XVIII.—The Geological Structure of North-East Northumberland. *Earth Environ. Sci. Trans. R. Soc. Edinb* 65, 449–481. doi:10.1017/S0080456800012709
- Stabler, C. L. (1968). Simplified Fourier analysis of fold shapes. *Tectonophysics* 6, 343–350. doi:10.1016/0040-1951(68)90049-8
- Stampfli, G., Marcoux, J., and Baud, A. (1991). Tethyan margins in space and time. *Palaeogeogr. Palaeoclimatol. Palaeoecol.* 87, 373–409. doi:10.1016/0031-0182(91)90142-E
- Stocklin, J. (1974). *Northern Iran: Alborz mountains, mesozoic – Cenozoic orogenic belt, data for orogenic studies*. London: Geological Society. *Special Publications* 4.
- Stocklin, J. (1968). Structural History and Tectonics of Iran: A Review. *Am. Assoc. Pet. Geol. Bull.* 52, 1229–1258. doi:10.1306/5D25C4A5-16C1-11D7-8645000102C1865D
- Tavarnelli, E., Holdsworth, R. E., Clegg, P., Jones, R. R., and McCaffrey, K. J. W. (2004). The anatomy and evolution of a transpressional imbricate zone, Southern Uplands, Scotland. *J. Struct. Geol.* 26, 1341–1360. doi:10.1016/j.jsg.2004.01.003
- Tirrul, R., Bell, I. R., Griffis, R. J., and Camp, V. E. (1983). The Sistan suture zone of eastern Iran. *Geol. Soc. Am. Bull.* 94, 134–150. doi:10.1130/0016-7606(1983)94<134:TSSZO>2.0.CO;2
- Torremans, K., Muchez, P., and Sintubin, M. (2014). Mechanisms of flexural flow folding of competent single-layers as evidenced by folded fibrous dolomite veins. *J. Struct. Geol.* 69, 75–90. doi:10.1016/j.jsg.2014.10.002

- Twiss, R. J. (1988). Description and classification of folds in single surfaces. *J. Struct. Geol.* 10, 607–623. doi:10.1016/0191-8141(88)90027-2
- Twiss, R. J., and Moores, E. M. (2007). *Structural geology* Second. W. H. Freeman.
- van Hise, C. R., and Hoskins, L. M. (1896). *Principles of north American pre-cambrian geology*. Washington: Gov't. Print. Off.
- Vernant, Ph., Nilforoushan, F., Hatzfeld, D., Abbassi, M. R., Vigny, C., Masson, F., et al. (2004). Present-day crustal deformation and plate kinematics in the Middle East constrained by GPS measurements in Iran and northern Oman. *Geophys J. Int.* 157, 381–398. doi:10.1111/j.1365-246X.2004.02222.x
- Walker, R., Jackson, J., and Baker, C. (2003). Surface expression of thrust faulting in eastern Iran: source parameters and surface deformation of the 1978 Tabas and 1968 Ferdows earthquake sequences. *Geophys J. Int.* 152, 749–765. doi:10.1046/j.1365-246X.2003.01886.x
- Walker, R. T., and Khatib, M. M. (2006). Active faulting in the Birjand region of NE Iran. *Tectonics* 25, 1–17. doi:10.1029/2005TC001871
- Walpersdorf, A., Manighetti, I., Mousavi, Z., Tavakoli, F., Vergnolle, M., Jadidi, A., et al. (2014). Present-day kinematics and fault slip rates in eastern Iran, derived from 11 years of GPS data. *J. Geophys. Res. Solid Earth* 119, 1359–1383. doi:10.1002/2013JB010620
- Wu, Y., Eckert, A., Liu, X., and Obrist-Farner, J. (2019). The role of flexural slip during the development of multilayer chevron folds. *Tectonophysics* 753, 124–145. doi:10.1016/j.tecto.2019.01.008
- Zang, A., and Stephansson, O. (2010). *Stress field of the Earth's crust*. doi:10.1007/978-1-4020-8444-7